RSC Advances

ROYAL SOCIETY OF CHEMISTRY

www.rsc.org/advances

In Vitro Evaluation of the Conjugations of Neonicotinoids with Transport Protein: Photochemistry, Ligand Docking and Molecular Dynamics Studies

Wei Peng,[abc] Fei Ding*[ad] and Yu-Kui Peng[e]

[a] *College of Agriculture and Plant Protection, Qingdao Agricultural University, Qingdao 266109, China*

[b] *College of Food Science and Engineering, Qingdao Agricultural University, Qingdao 266109, China*

[c] *Department of Chemistry, China Agricultural University, Beijing 100193, China*

[d] *Department of Biological Engineering, Massachusetts Institute of Technology, Cambridge, MA 02139, United States*

[e] *Center for Food Quality Supervision & Testing, Ministry of Agriculture, College of Food Science & Engineering, Northwest A&F University, Yangling 712100, China*

*Corresponding Author
Phone/fax: +86-29-87092367
E-mail: alexf.ting@outlook.com, feiding@cau.edu.cn

ABSTRACT

The main objective of this effort was to assess the biological effects of neonicotinoids, together with the structure-activity relationships, by employing plasma albumin as a nontarget model. Fluorescence indicated clearly that static type is the effective mechanism for the reduction of Trp-214 residue emission when c(neonicotinoid)$\leqslant$10 μM, yet both static and dynamic properties occurred in the system if the concentration is higher than 10 μM. The stoichiometric proportion of the protein-neonicotinoid is obviously at 1∶1, and subdomain IIA was discovered to possess high-affinity for these chemicals. This corroborates molecular docking, site-directed mutagenesis, molecular dynamics simulation and free energy calculation laying the neonicotinoids at the warfarin-azapropazone site, and yield hydrogen bonds, π-π stacking and hydrophobic interactions with several pivotal amino acid residues, i.e. Phe-211, Trp-214 and Arg-222. These noncovalent bonds caused partially conformational changes on protein, that is, the α-helix content was decreased from 55.9% to 48.5% along with an increase in the β-sheet, turn and random coil, as derived from synchronous fluorescence and circular dichroism. And this phenomenon squares well with the outcomes of the assignment of protein secondary structure. According to the analyses of structure-activity relationships, it can be observed that the neonicotinoids with the ring-closing structure (part B), e.g. imidacloprid and thiacloprid, have relatively low affinity toward protein, as compared with some ring-opening agents such as nitenpyram and acetamiprid. These disparities may be

referable to the fact that the ring-opening neonicotinoids hold great flexibility, and then generate noncovalent interactions with the amino acid residues in the active cavity more easily. In addition, toxicological relevance of the biorecognitions of neonicotinoids with biopolymer was also explored herein. Perhaps this exploration could use as a nontarget biological model for the evaluation of neonicotinoids toxicity and it might also provide helpful clues for the synthesis of novel neonicotinoids agents.

KEYWORDS: *neonicotinoids, globular protein, molecular dynamics simulation, free energy calculations, structure-activity relationships, toxicological relevance*

INTRODUCTION

Over the last few decades, the development of neonicotinoids as an importantly novel insecticide represents a milestone in agrochemical research. They are the only major new class of insecticides developed during these years.[1] For the moment the commercial neonicotinoids include acetamiprid, clothianidin, dinotefuran, imidacloprid, nitenpyram, sulfoxaflor, thiacloprid and thiamethoxam. Because of their low use dose and excellent activities on diverse types of pests, neonicotinoids account for approximately 20% of the global insecticides market and profit one billion dollars worldwide per year, especially imidacloprid.[2,3]

In fact, previous efforts clearly show that the neonicotinoids have good selectivity for the nicotinic acetylcholine receptors (nAChRs) in insects.[4,5] Nevertheless, molecular recognition of these agrochemical compounds to mammalians is very scarce. Regrettably, accumulatively toxicological data indicated that exposure to neonicotinoids may relate closely with the enriched production of terrible consequences in animals and perhaps humans.[6-9] Further, the available literatures on neonicotinoids and their degradation in mammalians have demonstrated that some of them can cause carcinogenesis, hepatotoxicity and probable teratogenicity.[10-12] Bhardwaj et al.[13] observed moderate pathological changes in female *Rattus norvigicus* Wistar rats administered 0, 5, 10, and 20 mg/kg/day by feed imidacloprid in corn oil for 90 days. Bal et al.[14] found that low doses of imidacloprid could lead to the deterioration in sperm motility and abnormality in sperm morphology in adult male

Wistar albino rats. After three months of oral fed of imidacloprid (8.0 mg per kilogram body weight), the apoptosis of germ cells has increased, and with seminal DNA fragmentation. Some experiments also proved that a number of widely used pesticides, including neonicotinoids, might arouse a panic for their probable endocrine disruptor property, which would eventually produce detrimental outcomes to grow up reproductive system in humans.[15,16] Moreover, Gawade et al.[17] and Devan et al.[18] alluded that continuous exposure to imidacloprid and acetamiprid during development will result in negative effects on immune system, and proposed that caution shall be taken to protect human beings, in particular, vulnerable persons such as children and pregnant women, from neonicotinoids.

Besides the toxicological problems, nowadays the issues of pesticide residues have emerged as the great anxiety as well.[19,20] Imidacloprid, which is currently the most extensively applied neonicotinoid insecticide in the world, has a relatively high water solubility (0.61 g L^{-1}) and degrade slowly in the environment.[21] If in soil under aerobic conditions, it can persist with a half-life ranging from 1 to 3 year and the content has almost doubled every 5 years since 1990s.[22,23] The widespread residues of neonicotinoids in the environment may have made matters worse and could induce the serious hazards to human health directly in the near future. Thereby it is most urgent that the comprehensive assessment of the toxicological action of neonicotinoids, notably by employing vitally multifunctional macromolecules such as enzymes/proteins or nucleic acids as the biological models should be executed.

In recent years, except for the *in vivo* experimental approaches, the biological

estimation of molecular recognition of various ligands with biopolymers, e.g. DNA, RNA, polypeptides and proteins is an essential part to receive a good comprehension of toxicological features.[24,25] Albumin, which is formed in the liver, is the most abundant protein in blood plasma and contributes nearly half of the blood serum protein. One of the interestingly biological functions of albumin is to transport endogenous and exogenous substances such as agrochemicals, bilirubin, colorants, fatty acids, hormones, metal ions and bioactive compounds.[26,27] Meantime, albumin account for most of the antioxidant capacity of plasma, and exhibit some types of enzymatic properties. Consequently, researchers use this protein as an excellent biomarker to evaluate many diseases involving cancer, ischemia, postmenopausal obesity and rheumatoid arthritis.[28] In addition, it has the ability to treat several diseases that might need to monitor the glycemic control. It is commonly accepted today that the degree of biointeractions between biopolymers and ligands would govern their absorption and dispersion into cellular tissues, affect their excretion from the living organism, and eventually influence substance's pharmaceutical and toxicological roles.[29,30] Thereby the exploration of the potentially adverse effects of neonicotinoids through utilizing albumin as a target is completely suitable, and this kind of study could provide pivotal clues in the structural aspects that consider the overall toxic activities of neonicotinoids.

To date many biophysical techniques have been used to check the ligand recognition events, including calorimetry, chromatography, crystallology, electrophoresis, equilibrium dialysis, fluorescence, light scattering, nuclear magnetic

resonance, surface enhanced Raman spectroscopy, surface tension, ultracentrifugation, ultrafiltration, etc.[31-33] Among them, fluorescence spectroscopy has been confirmed to be one of the most integrally qualitative and quantitative ways to analyze the noncovalent biomacromolecule-ligand reactions.[34] Nonetheless, molecular modeling can often be used to demonstrate the binding interactions via reasonably computational calculation, and it is also usually utilized to scrutinize the quantitative structure-affinity relationships.[35] In two more recently qualitative investigations, Mikhailopulo et al.[36] and Wang et al.,[37] respectively, probed the interactions between albumin and imidacloprid by steady-state fluorescence, but these works did not exposit the reaction essence, binding domain, structural changes, the key noncovalent bonds and the critical amino acid residues, etc. Very recently, we have preliminarily explored the biointeractions of imidacloprid and its major metabolites with some model biopolymers such as albumin from bovine serum, hemoglobin human and lysozyme from chicken egg white;[38,39] however, the precise recognition features, the concrete recognition location, conformational transitions, dynamic recognition processes, the binding free energies, structure-activity relationships of neonicotinoids and toxicological relevance are yet unresolved. These crucial information, particularly the dynamic reaction behaviors, may benefit our understanding of the biological toxicity and biotransformation of neonicotinoids in the human body.

Given the above-mentioned background, our current contribution was to deliberate the recognition nature, stoichiometry, binding location, structural transitions, dynamic interaction patterns along with the free energy in the presence of

neonicotinoids (structure shown in Fig. 1), by the combination of steady-state and time-resolved fluorescence, chemical denaturation, extrinsic 8-anilino-1-naphthalenesulfonic acid (ANS) probe, circular dichroism (CD), *in silico* docking, site-directed mutagenesis, molecular dynamics simulation as well as the decomposition of free energy. Specifically the structural-activity relationships and the toxicological relevance of neonicotinoids agents were further discussed in this attempt. Possibly this study will give beneficial understanding on dissecting the toxicological profiles of neonicotinoids, the relationships of structure and activity and the chemical essence of biorecognition between neonicotinoids and biological biomacromolecules.

Fig. 1 here about

EXPERIMENTAL

Material. Albumin from human serum (A3782, lyophilized powder, fatty acid free, globulin free, ≥ 99%), imidacloprid (37894, analytical standard) and 8-anilino-1-naphthalenesulfonic acid (A1028, ≥ 97%) employed in this assay were obtained from Sigma-Aldrich (St. Louis, MO) and utilized without further purification, and ultrapure water was prepared by a Super-Q® Plus Water Purification System from EMD Millipore Corporation (Billerica, MA). All of the experiments were conducted in Tris (0.2 M)-HCl (0.1 M) buffer of pH＝7.4, with an ionic strength of 0.1 in the existence of sodium chloride, and the pH was measured with an Orion Star A211 pH Benchtop Meter (Thermo Scientific, Waltham, MA). Albumin was stored in a

refrigerator at ~277 K, and dilutions of the albumin stock (10 μM) in Tris-HCl buffer solution were got instantly before application, the concentration of albumin was determined by the approach of Lowry et al.[40] All other chemicals used were of analytical reagent and acquired from Sigma-Aldrich.

Steady-State Fluorescence. Steady-state fluorescence spectra were collected with a 1.0 cm path length quartz cuvette applying a F-7000 Fluorescence Spectrophotometer (Hitachi, Japan) outfitted with a thermostatic bath. Both excitation and emission slits were fixed at 5.0 nm, fluorescence emission spectra were recorded by exciting the incessantly blended albumin at 295 nm to prefer tryptophan (Trp) fluorescence, and steady-state fluorescence were registered in the wavelength range of 300~500 nm at a scanning speed of 240 nm min^{-1}. The sample of blank involving of the Tris-HCl buffer solution of imidacloprid in relevant amounts was deducted from all fluorescence experiments.

Ligand Docking. Molecular docking of the albumin-neonicotinoids adducts was operated on SGI Fuel Visual Workstation-550L (Silicon Graphics International Corp., Milpitas, CA). The X-ray diffraction crystallographic structure of protein (entry codes 1AO6), solved at a atomic resolution of 2.5 Å,[41] was repossessed from the Research Collaboratory for Structural Bioinformatics (RCSB) Protein Data Bank (http://www.rcsb.org/pdb). After being input in the commercial software Sybyl Version 7.3 (http://www.certara.com), the structure of protein was thoroughly examined for atom and bond type exactness allocation. Hydrogen atoms were theoretically appended utilizing the menus of both Sybyl Biopolymer and Build/Edit.

To avert unfavorable amino acid/amino acid interactions and repellent steric conflicts, positions of hydrogen atoms only were energy minimized with the Powell's conjugate direction method with 0.05 kcal mol^{-1} energy gradient convergence criteria for 1,500 circulations, this action does not alter locations to heavy atoms, and the potential of the three-dimensional structure of protein was designated based upon the AMBER force field with Kollman charges. The two-dimensional configurations of neonicotinoids were obtained from the database of PubChem (http://pubchem.ncbi.nlm.nih.gov), and the original structures of these ligands were generated by the program of Sybyl 7.3.

Meanwhile, both hydrogen atoms and Gasteiger-Hückel partial charges were added and assigned for each neonicotinoid, respectively, and AM1-BCC charges[42] were also added to the insecticides imidacloprid and thiacloprid, respectively, in order to make sure the rationality of the added charges and further compare the differences between the two docking results. To validate the reasonableness of the initial docking conformation received by the Sybyl 7.3, the crystal structures contained imidacloprid (entry codes 3WTL) and thiacloprid (entry codes 3WTJ),[43] respectively, have been downloaded from the Protein Data Bank, and the ligand molecules gained from the two crystal structures will directly be docked to albumin. The irrationality of the original conformation induced by the addition of charges and force fields should be excluded, and the docking results were expressed in the form of superposition pictures.

The program of AutoDock 4.2,[44] which uses a fully automatic flexible molecular

199 docking algorithm, was employed to evaluate the possible conformation of the ligands
200 that binds to protein, and then the ligands would be docked to protein by utilizing a
201 Lamarckian Genetic Algorithm (LGA).[45] A grid box was defined before docking to
202 cover the entire system involving albumin and neonicotinoids with the size of 126
203 Å×126 Å×126 Å ($x \times y \times z$) with 0.56 Å grid spacing. A hybrid genetic algorithm
204 (i.e. LGA) has been used to ascertain the probable ligand binding location on protein.
205 All the generated conformations after docking were clustered up with tolerance of the
206 Root-Mean-Square Deviation (RMSD) of 2.0 Å from the structural candidates (20)
207 with the lowest energy. For each docking procedure, three conformations with the
208 lowest energy (RMSD＜1.0 Å) shall be overlaid so as to select the most suitable
209 docking conformation. And the computer program of PyMOL
210 (http://www.schrodinger.com), which is a user-sponsored molecular visualization
211 system, could ultimately be applied to exhibit the *in silico* docking results.

212 **Site-Directed Mutagenesis.** Site-directed mutagenesis processes were
213 accomplished by utilizing the module of "Mutate Monomers" in Sybyl Version 7.3,
214 and the Trp-214, Phe-211 and Arg-222 residues in albumin were respectively mutated
215 to alanine (Ala) residue which has nonaromatic and nonpolar properties. To guarantee
216 the stability of conformation, the mutated proteins were subjected to 3,000 simplex
217 minimization steps based on the AMBER force field with Kollman charges. Then the
218 molecular docking of mutated albumin-imidacloprid was run and the other parameters
219 were in full agreement with the above native albumin-imidacloprid complexation, and
220 the mutation results were further validated by using molecular dynamics (MD)

simulation.

Molecular Dynamics Simulation and the Decomposition of Free Energies. MD simulations of the native and mutated albumin-neonicotinoids were carried out using Gromacs program, version 4.5.5, with the Gromos96 ffG43a1 force field.[46,47] Simulation procedures were executed under physiological conditions (pH＝7.4), and the amino acid residues possessed acidity and basicity were adjusted to the protonation states at neutrality condition. Initial conformations of albumin and neonicotinoids were, respectively, taken from the original X-ray diffraction crystal structure that was measured at 2.5 Å resolution (entry codes 1AO6) and the optimal structures originated from molecular docking. The topology of albumin was yielded by Gromacs package directly, whereas neonicotinoids by PRODRG2.5 Server.[48] The simulation systems were solvated with a periodic cubic box (the volume is $7.335\times6.155\times8.119$ nm^3) filled with TIP3P water molecules and an approximate number (12) of sodium counterion to neutralize the charge.[49] Totally, there are 51,230 crystallographic solvent molecules, and the shortest distance between the complex and the edge of the box is set to 10 Å. Simulations were conducted utilizing the isothermal-isobaric (NPT) ensemble with an isotropic pressure of 1 bar, and the temperature of the neonicotinoids, albumin and solvent (water and counterion) was separately coupled to an external bath held at 300 K, using the Berendsen thermostat with 0.2 ps relaxation time.[50,51] The LINCS algorithm was employed to constrain bond lengths,[52-54] and the long-range electrostatic interactions beyond 10 Å were modeled using the Particle Mesh Ewald (PME) method with a grid point density of

0.1 nm and an interpolation order of 4.[55,56] A cutoff of 10 Å and 14 Å was used for Coulomb and van der Waals' interactions, respectively. The MD integration time step was 2.0 fs and covalent bonds were not constrained, and the system configurations were saved every 2.0 ps. To decrease the atomic collisions with each other, both gradient descent and conjugate gradient algorithms were utilized to optimize the whole system.[57,58] First the solvated starting structure was preceded by a 1,000 step gradient descent and then by conjugate gradient energy minimization. Subsequently, 100 ps equilibration with position restraints runs to remove possible unfavorable interactions between solute and solvent, and after thorough equilibration, MD simulations of the native protein-neonicotinoids and the mutational protein-neonicotinoid were, respectively, run for 30 ns and 50 ns. Further, the pure albumin was selected to operate 10 ns time period MD simulation and the outcomes of simulations were finally manifested via Visual Molecular Dynamics 1.9.2,[59] and the software Discovery Studio Visualization 4.5 (Accelrys, San Diego, CA) was used to display the pictures of the MD simulations. The program of Dictionary of Protein Secondary Structure (DSSP),[60,61] together with the tool of do_dssp embedded in Gromacs 4.5.5, was exploited to standardize secondary structure assignment in this study.

Additionally, the binding free energies for these molecular interactions were computed based on the following relationships:[62,63]

$$\Delta G_{bind} = G_{complex} - (G_{protein} + G_{ligand}) \quad (1)$$

$$\Delta G_{bind} = \Delta G_{gas} - \Delta G_{sol} \quad (2)$$

where

$$\Delta G_{gas} = \Delta H_{gas} - T\Delta S \approx \Delta E_{MM} - T\Delta S \quad (3)$$

$$\Delta G_{bind} \approx \Delta E_{MM} + \Delta G_{sol} - T\Delta S \quad (4)$$

$$\Delta E_{MM} = \Delta E_{\text{int}ernal} + \Delta E_{vdW} + \Delta E_{ele} \quad (5)$$

$$\Delta G_{sol} = \Delta G_{GB} + \Delta G_{SA} \quad (6)$$

$$G_{SA} = \gamma \times SASA + \beta \quad (7)$$

In these equations the binding free energy ΔG_{bind} is calculated from the contributions of gas phase energy ΔG_{gas} and solvation energy ΔG_{sol}, where ΔG_{gas} is composed of ΔE_{MM} and $T\Delta S$. The molecular mechanics energy (ΔE_{MM}) is comprised of the internal energy ($\Delta E_{\text{internal}}$), the van der Waals' energy (ΔE_{vdW}) and the electrostatic energy (ΔE_{ele}). The polar solvation component (ΔG_{GB}) is evaluated using the generalized Born method, and the nonpolar solvation component (ΔG_{SA}) is estimated utilizing solvent accessible area with the γ parameter set to 0.00542 kcal (mol Å)$^{-1}$ and the β parameter set to 0.92 kcal mol^{-1}, respectively. The Solvent Accessible Surface Area (SASA) is calculated using the linear combination of pairwise overlaps (LCPO) model. The error bar of the standard error (SE) is reckoned by

$$SE = \frac{STD}{\sqrt{N}} \quad (8)$$

where STD stands for the standard deviation and N is the number of trajectory snapshots.

RESULTS AND DISCUSSION

Tryptophan Fluorescence Studies. Basically, there are three amino acid residues with intrinsic fluorescence, i.e. phenylalanine (Phe), tryptophan (Trp) and tyrosine (Tyr), but only Trp and Tyr are utilized experimentally because their quantum yield is high enough to present a good fluorescence signal.[65] Therefore, intrinsic fluorescence of protein is frequently used to measure the association parameter, binding mode and rate constant of a specific binding equilibrium. To monitor the reaction between neonicotinoid and albumin, steady-state fluorescence of protein with various concentrations of neonicotinoid was acquired in Fig. 2. Intrinsic albumin fluorescence is normally owing to the emission of Trp residue when excited with 295 nm and the contributions from the Tyr residues could be ignored. Under the experimental conditions, neonicotinoid shows no fluorescence emission in the range 300～500 nm which did not interfere with protein fluorescence. Clearly, albumin displays a strong fluorescence emission peak at 338 nm following an excitation at 295 nm, and its intensity decreased regularly with the addition of neonicotinoid. These phenomena indicated that there was conjugation between protein and neonicotinoid, and the ligand situated in the region where Trp-214 located within or close the lone amino acid residue.[66] An analogous report has been portrayed by Bekale et al.[67] for the biorecognition of polyethylene glycols with milk β-lactoglobulin.

Fig. 2 here about

The sensitivity of indole fluorescence in protein is the central element in the variety of fluorescence observed between different proteins and ligands, and the study of fluorescence mechanism has been regarded as an effective method to inspect

protein dynamics and conformations. Fluorescence lifetime measurements have thus been employed to get the existence of disparate and distinctive protein conformations, and it can offer directly mechanistic information about the time dependence of the protein-ligand recognition processes. To clarify the essence of the albumin-neonicotinoid conjugation, the representative fluorescence decay patterns of protein at various molar ratios of neonicotinoid in Tris-HCl buffer, pH＝7.4, are appeared in Fig. S1 (Supporting Information), and the time-resolved fluorescence lifetime and their oscillations are also listed in Table 1. Evidently, the fluorescence decay curves matched nicely to a biexponential function kinetics, which may suggest the presence of conformers in equilibrium in the folded structure of albumin. As can be seen from Table 1, a short and a long lifetime is perceived to be τ_1＝3.14 ns and τ_2 ＝7.18 ns (χ^2＝1.09) for protein during the time-resolved fluorescence decay, respectively; while in the maximum concentration of neonicotinoid, the lifetime components are τ_1＝2.41 ns and τ_2＝6.31 ns (χ^2＝1.03). The biexponential decay in the present case might be ascribed to a single electronic transition of Trp residue, which could present as diverse conformational isomers in the protein. Actually, owing to steric effects between the side chain of Trp residue and the polypeptide backbone, all rotamers are not entirely possible.[68,69] The quenching group closest to the indole moiety is the small amino group after protein-neonicotinoid conjugate occurred, as a result, the rotamer with the maximum population and the fluorescence lifetime of 7.18 ns. Instead, if amino and carbonyl groups close to the indole ring, this rotamer can hold the small lifetime component of 3.14 ns. The decryptions of conformers of

protein are restricted to the solution, and the existence of different Trp residue rotamers has been strictly approved by nuclear magnetic resonance.[70,71] Hence, we have not tried to assign the separate constituents, but in contrast the average fluorescence lifetime has been used to gain a qualitative analysis. The average lifetime of protein reduces from 5.93 ns to 5.49 ns, at different neonicotinoid concentrations, illustrating evidently that the quenching of albumin Trp residue fluorescence by neonicotinoid is combind dynamic and static in nature, not just static or dynamic quenching. These results are in reasonable consonance with our following analyses based on steady-state fluorescence data by using the Stern-Volmer equation, and a comparable examination has been indicated by Abou-Zied et al.[72] for the interpretation of fluorescence quenching of protein in the presence of medicinal hydroxyquinoline chemicals, namely 6-hydroxyquinoline, 7-hydroxyquinoline and 8-hydroxyquinoline.

Table 1 here about

To elaborate the fluorescence quenching type, the well-known Stern-Volmer equation was used for emission data analysis, and the corresponding results fitted from Fig. 3 are summarized in Table 2. Usually, a linear Stern-Volmer plot is frequently suggestive of a single kind of fluorophores, all equivalently accessible to ligand. Intuitively, the Stern-Volmer plot Fig. 3 in such circumstance is an upward curvature, concave towards the *y*-axis. This outcome implied plainly that the fluorophore (Trp-214 residue) may be dwindled both by collision and by complex formation with the same compound (neonicotinoid). The Stern-Volmer plot seems to

be marked off into two periods, that is the concentration of neonicotinoid is less than or greater than 10 μM. The Stern-Volmer quenching constant $K_{SV,}$ in either case, is the opposite correlated with temperature, patently expressing the biointeraction between protein and neonicotinoid is controlled by static reaction in low concentration of ligand ($\leqslant$10 μM), whereas both static and dynamic is likely to predominate when the concentration exceeds 10 μM.

Fig. 3 here about

Table 2 here about

In pharmacology, as well as in toxicology, the association capacity is one of the most principal indicators when we estimate the potentially pharmacological or toxicological activities of a ligand such as specific drug or agrochemical for a biomacromolecule.[31] Knowledge of the recognition affinity has great significance in realizing of the absorption, distribution and bioavailability and even the quantitative depiction of dose-response relationship of a ligand.[73] The equation with a number (3) in Supporting Information has been employed to treat the raw steady-state fluorescence data, and Fig. S2 indicates the plots of $\log(F_0-F)/F$ *versus* $\log[Q]$ for the protein-neonicotinoid mixture at different temperatures and the corresponding results of K and n values were also collected in Table 2. Visibly, the association constant K in both low and high concentration of neonicotinoid is reduced with the rising temperature, which hinted the emerging of a weak adduct in the association process and the noncovalent conjugate might probably be in part decomposed when the temperature elevated. A primary cause for this phenomenon is that higher

temperature will typically result in the dissociation of weakly bound protein-ligand adducts, and consequently smaller amounts of static quenching.

According to the idea from Dufour and Dangles,[74] and also united several recent publications on the topic of biopolymer-ligand, e.g. diverse drugs, emodin, flavonoid and long-chain perfluoroalkyl acids,[75-78] it is quite clear that the complexation of neonicotinoid with albumin belongs to moderate affinity with respect to the other strong protein-ligand complexes with association constants ranging from 10^6 to 10^8 M^{-1}. In the light of the thermodynamic equation $\Delta G° = -RT\ln K$, we may compute the Gibbs free energy $\Delta G° = -5.67$ kcal mol^{-1} (298 K), which displays that the formation of protein-neonicotinoid was an exothermic reaction. Moreover, the value of n is approximately equal to 1, insinuating the presence of just one single binding site in protein for neonicotinoid. As noted earlier, a unique quality of intrinsic fluorescence of albumin is due to the Trp-214 residue at the subdomain IIA, from the value of n, neonicotinoid binding patch most likely close to this aromatic amino acid residue and yielding fluorescence quenching in the conjugation.

To verify the stoichiometry between neonicotinoid and protein estimated from the above discussion, the method of continuous variation (Job's plot) is adopted here to determine the stoichiometry. In this approach, the total molar concentration of neonicotinoid and protein are held fixed, but their molar fractions are varied.[79] Fluorescence emission spectra that is proportional to complex formation is plotted *against* the molar fractions of these two components, and the maximum on the plot corresponds to the stoichiometry of the two species. The Job's plot for

protein-neonicotinoid fluorescence at 338 nm upon excitation at 295 nm is shown in Fig. 4 and, apparently, the *x*-coordinate at the maximum in the curve is 0.509. This supports the 1∶1 protein-ligand complexation, and is perfectly in harmony with the above result derived from the double-logarithmic plots.

Fig. 4 here about

Structural Alterations. As has been shown, time-resolved fluorescence indicates the conformation of albumin is likely to change so as to accommodate neonicotinoid suitably through noncovalent bonds. The following content will primarily be centered on the identification of the structural changes of protein in the presence of neonicotinoid. To begin with, synchronous fluorescence method was used to characterize the conformation of albumin interfered with neonicotinoid. It contains parallel scanning of both excitation and emission monochromators whereas keeping a fixed wavelength gap ($\Delta\lambda$) or constant augmentation of energy (Δv) between them.[80] In Miller[81] and Burstein et al.[82] pioneering work, when $\Delta\lambda$＝15 nm or 60 nm, the distinctive characters of Tyr and Trp residues was acquired. Fig. 5 manifests the spectral intensity of synchronous fluorescence of albumin in Tris-HCl buffer solution in the existence of various concentrations of neonicotinoid. It is visible that the maximum fluorescence emission wavelength has a slight red shift at the investigated concentration range when $\Delta\lambda$＝60 nm, however, almost no shift when $\Delta\lambda$＝15 nm. The bathochromic effect denotes that the polarity around Trp residue was increased and the hydrophobicity was decreased. That is to say, neonicotinoid is within easy reach of the Trp-214 residue, and then has remarkable impact on the Trp-214 residue

419 microenvironment nearby. Nevertheless, the synchronous fluorescence intensity
420 declined regularly with the addition of neonicotinoid, which further demonstrated the
421 occurrence of fluorescence quenching in the association reaction.

422 Fig. 5 here about

423 Circular dichroism (CD), particularly far-UV CD is an important tool in structural
424 biology for examining the folding, kinetics and whether protein-protein or
425 protein-ligand interactions alter the conformation of protein. If there are any
426 conformational changes, this event can lead to a spectrum which will differ from the
427 sum of the individual portions. To quantitative analyze the structural alterations of
428 globular protein, the experiments of CD spectra of protein in the absence and presence
429 of insecticide were recorded in Fig. S3 and the components of secondary structures
430 calculated based on raw CD data also illustrated as follows. The CD curve of albumin
431 showed two minus bands in the far-UV CD area at 208 nm and 222 nm, feature of
432 α-helical configuration of globular protein. The sensible clarification is that the
433 negative peaks between 208 nm and 209 nm and 222 nm and 223 nm are both
434 originated from $\pi \rightarrow \pi^*$ and $n \rightarrow \pi^*$ transition for the peptide bond of α-helix.[83] Free
435 protein possess 55.9% α-helix, 8.1% β-sheet, 11.6% turn and 24.4% random coil,
436 upon interact with neonicotinoid, decline of α-helix structure was viewed from 55.9%
437 free albumin to 48.5% albumin-neonicotinoid complex; whereas increase in β-sheet,
438 turn and random coil from 8.1%, 11.6% and 24.4% free albumin to 9.2%, 14.2% and
439 28.1% albumin-neonicotinoid at a molar ratio of albumin to pesticide of 1∶8. The
440 decrease of α-helix with a growth in the β-sheet, turn and random coil interprets the

441 neonicotinoid interacted with some residues of the peptide chain and eventually
442 produces the disturbance of the albumin three-dimensional structure, e.g. some degree
443 of biomacromolecule destabilization upon neonicotinoid complexation.[84] These
444 experimental facts may further attest the previous speculation by Mikhailopulo et al.[36]
445 that the conformation of protein would be disrupted through the noncovalent
446 protein-ligand recognition.

447 All of the above measurements and illustrations ratified the biorecognition of
448 neonicotinoid with albumin aroused conformational perturbations in protein, which
449 could probably be related to its physiological function. It is worthwhile to note that
450 the unfolding of albumin in this part does not signify the pesticide caused widespread
451 destruction of the three-dimensional structure of protein. Because albumin in solution
452 might usually be deemed as endowing a single shape overall, but it is possibly more
453 authentic to consider it as an assembly of peristaltic, flexible parts and frequently
454 altering in conformation via opening and closing of chief fissures.[85,86] With this mode
455 of alteration, together with many of its amino acid side chains incessantly in motion
456 on a microscale sphere, all of these make albumin well adapted to soak up or veer out
457 the many substances such as insecticide that it carries in the human body.

458 **Molecular Docking.** Molecular docking can suitably be used to investigate the
459 complexation of ligand at the active site of receptor. In the current study, this method
460 was applied to examine the binding of neonicotinoids at the active domain of protein.
461 Albumin is one of the most studied model proteins since its high-resolution tertiary
462 structure has been solved through X-ray diffraction crystallography by He and

Carter[87] in 1992. According to the atomic analysis of crystallized albumin, it is a heart-shaped tridomain protein which consists of 585 amino acid residues, and each domain is a product of two subdomains that hold conjunct structural motifs. The three domains, although homologous, have dissimilar ligand binding functions. Prior to explain the docking results, the influences of the two force fields, i.e. Gasteiger-Hückel partial charges and AM1-BCC charges, on the outcomes of molecular docking have been interpreted by using superposition pattern in this text, and the data are clearly revealed in Fig. 6. The results displayed that the addition of Gasteiger-Hückel partial charges and AM1-BCC charges has little impact on the docking results, and the superimposed data also suggested that the optimal conformations have high comparability. Meantime, via overlaying multiple low energy conformations in the present four docking systems, we could find some subtle differences, but undoubtedly, the optimal conformations may satisfactorily be superimposed on the most low energy conformations which have similar energy with the best conformations.

Fig. 6 here about

The best docking energy outcome ($\Delta G° = -5.87$ kcal mol^{-1}) of the protein-imidacloprid adduct is exhibited in Fig. 7. As can be seen from Fig. 7, the two oxygen atoms of the nitryl in imidacloprid can make hydrogen bonds with the hydrogen atom of amino group and the hydrogen atom of the secondary amine in Arg-222 residue, and the bond lengths are 2.05 Å and 2.47 Å, respectively. Furthermore, the molecular distance between the center of the pyridine ring in ligand

485 and the core of the indole ring in Trp-214 and the benzene ring of Phe-211 residues
486 are 3.14 Å and 3.27 Å, accordingly indicating that distinct π-π stacking, which looks
487 like a "sandwich", also occurred between albumin and imidacloprid. In the light of
488 surface modification of protein, we perceived that the entire neonicotinoid is towards
489 the hydrophobic pocket that is constituted of Phe-211, Trp-214, Ala-215, Leu-219,
490 Leu-238 and Val-343 residues, confirming that hydrophobic interactions worked
491 between them. Meanwhile, the optimal docking results of other
492 protein-neonicotinoids (thiacloprid, nitenpyram and acetamiprid) complexes are
493 emerged in Fig. 13, and the critical noncovalent interactions would be illuminated in
494 the following part of structure-activity relationships.

495 Fig. 7 here about

496 Site-directed mutagenesis is a powerful research tool used to study the structure
497 and function of enzyme/protein, especially some crucial amino acid residues and the
498 central noncovalent interactions generated by these residues in biopolymer. To further
499 confirm these key forces in the noncovalent protein-neonicotinoid process, the amino
500 acid residues – Trp-214, Phe-211 and Arg-222 have been chosen based on the above
501 explications, and site-directed mutagenesis experiments of these residues will be
502 conducted herein. In the following content, we describe the mutation of Trp-214
503 residue in detail, and the phenomena of mutation of Phe-211 and Arg-222 residues
504 might be elaborated on Supporting Information. The result of mutated
505 protein-imidacloprid reaction is displayed in Fig. 8, we noticed that the hydrogen
506 bonds between the oxygen atoms of polar nitryl in imidacloprid and the hydrogen

atom of the hydroxyl group in Ser-202 residue were clearly weakened, and the bond lengths are found to be 2.32 Å and 2.84 Å. Meantime, although the π-π stacking disappeared after the mutation of Trp-214 residue, weak hydrophobic interactions remained in the mutated system, and these residues includes Phe-211, Ala-213, Ala-214, Ala-215, Leu-219, Leu-238 and Val-343. Significantly, the noncovalent strength of the whole system has a downward tendency, such evident changes can be attributed to the mutation of residue tryptophan (Trp) to alanine (Ala), which decreases obviously the noncovalent interactions between the amino acid residues situated within the active region and neonicotinoid.

Fig. 8 here about

Molecular Dynamics Simulation and Free Energy Calculations. Molecular dynamics (MD) simulation capture the behavior of biomacromolecules in full atomic detail, and this method could thereby help to substantiate the accuracy of the docking results. Meanwhile, these dynamic data may assist us in seeking the energy changes of the biopolymer-ligand systems in a short time frame, and then provide important information for the decomposition of free energies.[88,89] To affirm the conformational stability of the protein-neonicotinoids under simulated physiological conditions, and further earn the binding free energies of the noncovalent complexes, MD simulations were performed for the four protein-ligand conjugates. In the present attempt, the complexed conformation received from molecular docking was used as the initial conformation for MD simulation, and the simulation time for the native protein-neonicotinoids is 30 ns. Nevertheless, the pure protein was also executed 10

ns simulation process. Frequently, if the fluctuation of the RMSD value for a typically dynamic system keeps within 0.1 nm, the system can be regarded as the actualization of a stably dynamic equilibrium state. It is quite evident from Fig. 9 that the four noncovalent protein-neonicotinoids adducts might be equilibrated within the time period of 5,000 ps, whereas the pure protein may reach the equilibrium state at the time point of 2,000 ps.

Fig. 9 here about

Nonetheless, MD simulations of the mutated protein-neonicotinoid complexes have also been executed so as to prove the rationality and stability of binding pattern regarding the mutated amino acid residues (Trp-214, Phe-211 and Arg-222) on protein and neonicotinoid. As regards the three mutated systems, that is protein (Trp-214→Ala-214)-imidacloprid, protein (Phe-211→Ala-211)-imidacloprid and protein (Arg-222→Ala-222)-imidacloprid, simulation processes have respectively been conducted with the time length of 50 ns. We can find these mutated protein-ligand systems could achieve the dynamic equilibrium state before 8,000 ps. The variation tendency of noncovalent interactions between mutated protein and neonicotinoid under physiological conditions might be deciphered via the dynamic data. Fig. 10 denotes the RMSD changes of conformations of molecular docking, concerning the mutated protein-imidacloprid adducts in the MD simulation. Apparently, if we mutate Trp-214 residue to Ala residue in the polypeptide chain, the mutated protein-imidacloprid system began to stabilize in the 1,500 ps. The backbone C_α atoms of mutated protein (black) fluctuates stably at 0.4 nm, and the amplitude is

within a range of 0.1 nm; while the RMSD of imidacloprid (red) oscillates at about 0.15 nm, and the undulate range should be within 0.05 nm. As for the other mutated protein-imidacloprid adducts, i.e. Phe→Ala and Arg→Ala residues, the MD simulation of these conjugates and careful elucidation of dynamic results may be revealed on the Supporting Information.

Fig. 10 here about

To inspect whether the binding conformation in dynamic equilibrium can match the results of molecular docking, the average conformation between 2,000 ps and 8,000 ps time frame was selected and superimposed on the initial conformation of MD simulation, and the outcome is presented in Fig. 11. It is very clear that the original conformation of the mutated protein-neonicotinoid adduct overlaps the equilibrium conformation completely, and the alterations in binding mode between mutated protein and neonicotinoid are rather small, the fluctuation of RMSD mainly roots in the overall translation of the complex. Although there are no obvious changes in binding style and conformation, it is noteworthy that the downward trends are observable in hydrogen bonds between Ser-202 residue and imidacloprid. The equilibrium conformation of MD simulation shows the oxygen atoms of nitryl in imidacloprid could make hydrogen bonds with the hydrogen atom of hydroxyl group in Ser-202 residue, and the bond lengths are 2.41 Å and 3.15 Å, respectively. This means that the mutation of Trp-214 residue shall be a trigger for the decrease of affinity between protein and neonicotinoids, or rather, the residue Trp-214 is extremely important in the protein-neonicotinoids reactions.

573 Fig. 11 here about

574 Integrative contrast of the recognition characters between native and mutated
575 protein, we may reasonable draw the conclusion that the mutation of some crucial
576 amino acid residues such as Trp-214, Phe-211 and Arg-222 will not only evoke the
577 changes of hydrogen bonds, but also cause the decrease and disappearance of
578 conjugated effects and hydrophobic interactions. These issues would remarkably
579 reduce the noncovalent strength between protein and neonicotinoid. Accordingly,
580 there is no doubt that residues Trp-214, Phe-211 and Arg-222 play an essential role in
581 the molecular recognition of neonicotinoids by plasma albumin.

582 In the same instant we might allocate the secondary structure constituents of
583 protein in the native and mutated states by the combination of DSSP and Gromacs
584 programs, and the results of α-helix, β-sheet and turn are displayed in Table 3.
585 Distinctly, secondary structure assignments based on dynamic data suggests that free
586 protein has a relatively high 54.1% α-helix, 10.3% β-sheet and 10.7% turn content;
587 upon imidacloprid complexation, major reduction of α-helix was observed from
588 54.1% free protein to 44.3% in protein-imidacloprid, and an increase in the β-sheet
589 and turn structures was also detected from 10.3% and 10.7% free protein to 12.7%
590 and 13.5% in protein-imidacloprid, respectively. According to the wet experiments of
591 far-UV CD, free protein in solution contains 55.9% α-helix, 8.1% β-sheet and 11.6%
592 turn, while the secondary structures of protein were changed to 48.5% α-helix and
593 9.2% β-sheet and 14.2% turn after imidacloprid interaction. One could find that the
594 secondary structures estimated from both far-UV CD spectra and MD simulations are

595 closely similar, and consequently this phenomenon testifies that the results of
596 molecular modeling are fully reliable in the current context.

597 Table 3 here about

598 The free energy is a basic quantity narrating the stability of a system because the
599 free energy of a system is minimized if the system is at equilibrium with its
600 environment, thereby evaluating the free energy is highly useful in simulations of
601 biological systems.[90] Frequently, the method of Molecular Mechanics/Generalized
602 Born Surface Area (MM/GBSA) has been applied to a variety of biomolecular
603 computational problems including receptor-ligand recognition.[91,92] According to the
604 previous data of MD simulations, the calculations of free energy of the last 10 ns
605 dynamic processes in equilibrium state have been proceeded by employing
606 MM/GBSA approach, and the time interval is 2.0 ps. As indicated distinctly in Table 4,
607 the energies derived from the MM/GBSA have some discrepancies with the results
608 from molecular docking, but the variation trends of energies are in accord with the
609 analyses of molecular docking, and the sequence is detected to be thiacloprid＜
610 imidacloprid＜acetamiprid＜nitenpyram. The binding free energy values evinced that
611 the most favorable interaction energies inhered in the protein-nitenpyram (ΔG_{bind}＝－
612 7.24 kcal mol^{-1}), and the differences of the van der Waals' energies (ΔE_{vdW}) of the
613 four noncovalent systems are relatively small, whereas the electrostatic energies
614 (ΔE_{ele}) have some notable disparities. This may well be the crucial reason that leads to
615 the generation of free energy differences for the neonicotinoid agents. Comparison
616 with the hydrophobicity discrepancies between the nonpolar solvation and ligand

molecules, one can notice that the stronger the hydrophobicity of the ligand, the lower the ΔG_{SA} value. However, as for the mutated protein-neonicotinoid, the free energies received from molecular dockings and MD simulations are slightly larger than the native protein-neonicotinoid adducts. These events further support the former view that the Trp-214, Phe-211 and Arg-222 residues are vitally important to the biopolymer-neonicotinoids recognition.

Table 4 here about

Structure-activity Relationships. According to the preceding explorations, the commercial and potential neonicotinoids are commonly constituted of three structural elements (structure shown in Fig. 12). Among them, imidacloprid, thiacloprid, nitenpyram and acetamiprid display some similarity that they all have 4-substituted chloropyridinyl group in their structure.[2,93,94] However, imidacloprid and thiacloprid contain heterocyclic spacer in part B, on the contrary, nitenpyram and acetamiprid include acyclic spacer on the element. Chemically, the modification of substituent group on B component might hold the potential to affect the biorecognition between protein and neonicotinoids. To authenticate this point, the neonicotinoids, viz. thiacloprid, nitenpyram and acetamiprid, have been selected for performing ligand docking studies, and the best results are exhibited in Fig. 13.

Fig. 12 here about

Fig. 13 here about

Obviously, the free energies of the protein-nitenpyram ($\Delta G_{bind}/\Delta G_{docking}$ = −7.24/−6.69 kcal mol^{-1}) and the protein-acetamiprid ($\Delta G_{bind}/\Delta G_{docking}$ = −6.50/−6.11 kcal

639 mol^{-1}) are larger than the protein-imidacloprid, one logical explanation is that the
640 critical noncovalent bonds such as hydrogen bonds between the two
641 protein-neonicotinoid complexes are stronger than the protein-imidacloprid adduct.
642 The oxygen atom and the nitrogen atom of nitryl and the hydrogen atom of the
643 secondary amine in the acyclic spacer of nitenpyram, could form hydrogen bonds
644 with the hydrogen atom of amino group in Arg-222 and the nitrogen atom of the
645 imidazole ring in His-242 residues, and the bond lengths are, respectively, 2.07 Å,
646 3.06 Å and 2.28 Å (Fig. 13(A)). This pattern will make the conformation of
647 nitenpyram more stable at the active cavity on protein molecule. As a result, the
648 recognition ability of acetamiprid with protein is lower than nitenpyram, but still
649 better than imidacloprid.

650 With regard to the protein-acetamiprid (Fig. 13(B)), the nitrogen atom of the
651 cyano group in acetamiprid may yield two hydrogen bonds with the hydrogen atoms
652 of the amino group and the secondary amine in Arg-222 residue, and the bond lengths
653 are 2.03 Å and 2.29 Å, respectively. Both bond lengths and affinity supports the
654 deduction that the toxicity of acetamiprid was greater than its analogous imidacloprid.
655 While for the protein-thiacloprid ($\Delta G_{bind}/\Delta G_{docking}$ = −4.22/−5.13 kcal mol^{-1}), which
656 has the same constituent – heterocyclic group as imidacloprid in B spacer, the reaction
657 of thiacloprid with protein is worst compared with that with the other neonicotinoids,
658 and the best recognition profile is also exposed in Fig. 13(C). It is conspicuous that
659 thiacloprid can not generate hydrogen bond with biomacromolecule, however, the π-π
660 stacking existed between the pyridine ring in thiacloprid and the benzene ring in

Phe-211 and the indole ring in Trp-214 residues. This event should enable the neonicotinoid to stay at the functional domain. On the basis of the structure-activity discussions, we might understand that the two neonicotinoids – nitenpyram and acetamiprid with acyclic spacer possess higher affinity and larger noncovalent interactions than imidacloprid and thiacloprid with heterocyclic substituents.

Probably these recognition disparities spring from the molecular flexibility of the neonicotinoids. Actually, the flexibility of heterocyclic segment is less than acyclic fragment in insecticides, the polar functional groups, that is nitryl and cyano groups in nitenpyram and acetamiprid, respectively, would yield excellent noncovalent bonds with the surrounding amino acid residues, and in consequence this feature could form more forceful association interactions, as compared with imidacloprid and thiacloprid. Such phenomenon can expound the discrepancy of biomolecular recognition of neonicotinoids by biopolymer, and we also believe that the properties of substituents in neonicotinoids may act a fundamental role in the macromolecule-pesticide biorecognition. Furthermore, these issues offers theoretical foundation to our previous opinion, namely a neonicotinoid with high binding strength to protein shall own a longer half-life, which can enhance the toxicity of the agrochemical for human health.

Toxicological Relevance. To explore the relationships between the molecular structures of the four typical neonicotinoid insecticides and the possibly noxious effects in great detail, the physicochemical and toxicological data of these neonicotinoids have been assessed based upon the authoritative tools such as VEGA,[95] Estimation Program Interface (EPI) Suite and Toxicity Estimation Software

683 Tool (TEST),[96,97] which developed by the European Environment Agency and the U.S.
684 Environmental Protection Agency, and the results were collected in Table 5. Evidently,
685 nitenpyram possess strong hydrophilicity, this quality might largely be chalked up to
686 the ring-opening structure and multiple hydrophilic groups in the neonicotinoid.
687 While for acetamiprid, this compound still retains the ring-opening structure, but the
688 hydrophilic groups are limited, so acetamiprid has relatively high hydrophobicity.[98]
689 Additionally, nitenpyram has both carcinogen and developmental toxicant
690 characteristics, whereas the other neonicotinoids, that is acetamiprid, imidacloprid and
691 thiacloprid do not possess both carcinogen and developmental toxicant
692 simultaneously; conversely, either carcinogen or developmental toxicant could be
693 given on these neonicotinoids. Such facts are closely associated with the structural
694 features of neonicotinoids. As we expatiated in the structure-activity studies, the
695 noncovalent forces between protein and nitenpyram outweigh clearly the other three
696 neonicotinoids, as nitenpyram contains the representative ring-opening structure and
697 more polar groups. This research finding should also be unraveled the nitenpyram
698 may hold greater toxicity and carcinogenicity. Nevertheless, it is worth mentioning
699 that there are no very forceful correlations among acute toxicity, carcinogenicity and
700 mutagenicity, that is why nitenpyram has lower LC_{50} and LD_{50}, but the chronic
701 toxicity of this neonicotinoid is far higher than that of acetamiprid, imidacloprid and
702 thiacloprid.

703 Table 5 here about

704 Further, there are several exact evidences that imidacloprid might not be the most

toxic analogue among the commercial neonicotinoids, whereas nitenpyram and acetamiprid may own greater negative impact on the human body than imidacloprid. The haemato-biochemical and histopathological examinations in male Wistar rats has demonstrated that administration of acetamiprid for nearly one month will result in significant increase in alanine transaminase, aspartate transaminase, lactate dehydrogenase and creatinine kinase level in serum, and obvious decrease in hemoglobin and total erythrocyte count.[99] Meantime, individual cell necrosis and karyomegaly were observed in liver, and mild glomerular oedema, congestion and desquamated epithelial cells were also detected in kidney. As for female Wistar rats, the *in vivo* hematological study suggested that acetamiprid has adverse effect on hemopoietic organs in animals via subacute exposure.[100] And, the toxicological evaluation of imidacloprid noted similar changes in male rats, the result also implied that imidacloprid can lead to the reduction of acetylcholinesterase activity in brain. Still, Ford and Casida[93] denoted that the chloropyridinyl neonicotinoid insecticides are readily metabolized and excreted in male albino Swiss-Webster mice as well. The $t_{1/2}$ relative to the maximum level is much higher for acetamiprid ($>$240 min) than imidacloprid (80 min) and thiacloprid (50 min) in plasma.

For mammals, the neonicotinoids will chiefly be complexed with neuronal nAChR, and such biomolecular interactions may produce several pathological symptoms, for instance, neuronal apoptosis, differentiation, migration, proliferation and synapse formation.[101] Recent scientific achievements show that the neonicotinoids, including imidacloprid and acetamiprid, are absorbed and transported

by functional biomolecules (primarily albumin) in the organism, and then pass through the blood-brain barrier, and eventually bind to the target nAChR.[93,102] In the meantime the IC_{50} values of both imidacloprid and acetamiprid for mammalian neuronal nAChR are 2,600 nM and 700 nM, respectively, which signify that the biological effects of acetamiprid for nAChR should evidently be larger than imidacloprid.[103] In general, a substance with a high protein binding affinity might possess a long half-life ($t_{1/2}$), which would increase its toxicity. In contrast, a compound with a low protein binding affinity is restricted in its capacity to perfuse tissues and reach the location of action. As set forth, the overall noncovalent bond lengths of the protein-acetamiprid reaction are observed to be smaller than the protein-imidacloprid. This fact suggested distinctly that the association affinity of the protein-acetamiprid is higher than the protein-imidacloprid; in other words, the protein-acetamiprid adducts may exist in the body for quite a long time. In the circumstances more acetamiprid molecules can be delivered to neuronal nAChR via the active transporter (albumin) and ultimately engender greater toxic actions. These proofs shall hold common aspects with our formerly comprehensive explorations, and a neonicotinoid with more flexibility and could endow great recognition strength to nontarget biomacromolecules, which would increase its toxicity.

Aside from the parent compound of neonicotinoids, we should point out that these chemicals might be biodegraded by metabolic attack at different moiety. Maybe several metabolites, in some cases, contribute to the overall toxicities such as carcinogenesis and hepatotoxicity for mammalian. Recently, an interesting

749 scrutinization is endorsed by Casida[104] who have considered that we may get
750 opportunities for metabolic selectivity and programmed persistence if we can take the
751 wide diversity of neonicotinoid substituents into consideration. And finally obtain the
752 neonicotinoid pesticides that possess selective toxicity to various pests while
753 relatively safe to human beings and beneficial organisms.
754
755 **CONCLUSIONS**
756
757 To sum up, the current scenario unwrap the biorecognition events of the maximum
758 sold neonicotinoids with the multifunctional albumin by combining experimental and
759 computational techniques at the molecular scale. Data of fluorescence confirmed that
760 the decrease of Trp residue emission was originated from a static reaction in low
761 concentration of neonicotinoid, while both static and dynamic processes operated
762 when the concentration of neonicotinoid exceed 10 μM. The binding strength of
763 neonicotinoid with protein falls within the range of moderate affinity with the
764 stoichiometry of 1∶1, and the noncovalent bonds, such as hydrogen bonds, π-π
765 stacking and hydrophobic interactions, are largely responsible for stabilizing the
766 protein-neonicotinoid adduct. Moreover, GuHCl induced albumin denaturation,
767 extrinsic ANS fluorescence and site-specific competitive binding experiments were all
768 suggested that the subdomain IIA, Sudlow's site I, owned high-affinity for the binding
769 of neonicotinoid to protein. These outcomes are in concert with the molecular docking,
770 site-directed mutagenesis, MD simulation and the decomposition of free energy

771 placing the neonicotinoids in the warfarin-azapropazone site, and several amino acid
772 residues, i.e. Phe-211, Trp-214 and Arg-222 have a major role in the noncovalent
773 recognitions.

774 Time-resolved fluorescence decay illustrates the conformation of protein may be
775 yielded a slight transformation when neonicotinoid conjugated with protein. This
776 phenomenon has further been verified by synchronous fluorescence and far-UV CD
777 that the α-helix of protein was reduced from 55.9% to 48.5% with an increase in the
778 β-sheet, turn and random coil of the protein-neonicotinoid complex. And the results of
779 MD simulations validate the trends of conformational alterations in the presence of
780 neonicotinoids. Based on the structure-activity relationships, it can be assured that the
781 structural differences in part B of neonicotinoids could affect the recognition capacity
782 between protein and neonicotinoids. To be more exact, the ring-opening structure will
783 vest neonicotinoids in greater flexibility, and then it is more likely to produce
784 noncovalent bonds with amino acid residues during the protein-neonicotinoids
785 reactions. Perhaps this is the reason that the association abilities of nitenpyram and
786 acetamiprid with protein are higher than the ring-closing neonicotinoids, e.g.
787 imidacloprid and thiacloprid. Indeed the protein-neonicotinoids complexes are found
788 to be related closely to toxicological actions of these agrochemicals. Due to
789 neonicotinoids are one of the most widely used pesticides, along with the highly
790 controversial topic at present regarding the possible toxicity of these compounds for
791 nontarget mammalians, we hope this study might offer useful information for
792 evaluating potentially detrimental effects of the insecticides.

ASSICIATED CONTENT

Supporting Information

Detailed protocols of time-resolved fluorescence and extrinsic ANS displacement, site-specific ligand binding and CD spectra, principles of fluorescence quenching, evaluation of association ability, the discussions of ligand binding domain and the mutations of Phe-211 and Arg-222 residues, and the images of time-resolved fluorescence decays, association constant plot, far-UV CD spectra, fluorescence quenching pictures of albumin and ANS-albumin adduct as well as the colorful pictures of the mutations of Phe-211 and Arg-222 residues.

AUTHOR INFORMATION

Corresponding Author

*E-mail: alexf.ting@outlook.com, feiding@cau.edu.cn. Phone/fax: +86-29-87092367.

NOTES

The authors declare no competing financial interest.

ACKNOWLEDGEMENTS

We are greatly indebted to Professor Ulrich Kragh-Hansen of Department of Biomedicine, University of Aarhus, for the precious gift of his doctoral dissertation. We particularly appreciate Dr. Peter Ertl of Novartis Institutes for BioMedical Research (Basel, Switzerland) for his kindly supply of JME Molecular Editor. We thank Editors Jessie Morgan and Allison Holloway of Royal Society of Chemistry, for their warm support during the manuscript processing. Thanks also go to the reviewers of this manuscript for their constructive and insightful suggestions.

ABBREVIATIONS USED

Ala, alanine; ANS, 8-anilino-1-naphthalenesulfonic acid; Arg, arginine; CD, circular dichroism; DNA, deoxyribonucleic acid; DSSP, Dictionary of Protein Secondary Structure; EPI, Estimation Program Interface; GuHCl, guanidine hydrochloride; HCl, hydrochloric acid; His, histidine; IRF, instrument response function; LCPO, linear combination of pairwise overlaps; Leu, leucine; LGA, Lamarckian Genetic Algorithm; Lys, lysine; MD simulation, molecular dynamics simulation; MM/GBSA, Molecular Mechanics/Generalized Born Surface Area; nAChRs, nicotinic acetylcholine receptors; NPT, isothermal-isobaric; Phe, phenylalanine; PME, Particle Mesh Ewald; R, correlation coefficient; RCSB, Research Collaboratory for Structural Bioinformatics; RMSD, Root-Mean-Square Deviation; RNA, ribonucleic acid; SASA, Solvent Accessible Surface Area; S.D., standard deviation; Ser, serine; TEST, Toxicity

Estimation Software Tool; Tris, tris(hydroxymethyl)aminomethane; Trp, tryptophan; Tyr, tyrosine; UV/vis, ultraviolet-visible spectroscopy; Val, valine; VEGA, Virtual models for property Evaluation of chemicals within a Global Architecture.

REFERENCES

1. S. C. Kessler, E. J. Tiedeken, K. L. Simcock, S. Derveau, J. Mitchell, S. Softley, J. C. Stout and G. A. Wright, *Nature*, 2015, **521**, 74-76.
2. J. E. Casida and K. A. Durkin, *Annu. Rev. Entomol*., 2013, **58**, 99-117.
3. M. R. Douglas and J. F. Tooker, *Environ. Sci. Technol.*, 2015, **49**, 5088-5097.
4. T. T. Talley, M. Harel, R. E. Hibbs, Z. Radić, M. Tomizawa, J. E. Casida and P. Taylor, *Proc. Natl. Acad. Sci. U. S. A.*, 2008, **105**, 7606-7611.
5. P. Jeschke, R. Nauen and M. E. Beck, *Angew. Chem. Int. Ed.*, 2013, **52**, 9464-9485.
6. G. Di Prisco, V. Cavaliere, D. Annoscia, P. Varricchio, E. Caprio, F. Nazzi, G. Gargiulo and F. Pennacchio, *Proc. Natl. Acad. Sci. U. S. A.*, 2013, **110**, 18466-18471.
7. A. D. Ozsahin, R. Bal and O. Yılmaz, *Toxicol. Res.*, 2014, **3**, 324-330.
8. V. Doublet, M. Labarussias, J. R. de Miranda, R. F. A. Moritz and R. J. Paxton, *Environ. Microbiol.*, 2015, **17**, 969-983.
9. D. Goulson, E. Nicholls, C. Botías and E. L. Rotheray, *Science*, 2015, **347**, DOI: 10.1126/science.1255957.

10. S. L. Carmichael, W. Yang, E. Roberts, S. E. Kegley, A. M. Padula, P. B. English, E. J. Lammer and G. M. Shaw, *Environ. Res.*, 2014, **135**, 133-138.

11. K. V. Vinod, S. Srikant, G. Thiruvikramaprakash and T. K. Dutta, *Am. J. Emerg. Med.*, 2015, **33**, 310.e5-310.e6.

12. P. Bagri, V. Kumar and A. K. Sikka, *Drug Chem. Toxicol.*, 2015, **38**, 342-348.

13. S. Bhardwaj, M. K. Srivastava, U. Kapoor and L. P. Srivastava, *Food Chem. Toxicol.*, 2010, **48**, 1185-1190.

14. R. Bal, G. Türk, M. Tuzcu, O. Yilmaz, T. Kuloglu, R. Gundogdu. S. Gür, A. Agca, M. Ulas, Z. Çambay, Z. Tuzcu, H. Gencoglu, M. Guvenc, A. D. Ozsahin, N. Kocaman, A. Aslan and E. Etem, *J. Environ. Sci. Health B.: Pestic. Food Contam. Agric. Wastes*, 2012, **47**, 434-444.

15. M.-L. Jugan, Y. Levi and J.-P. Blondeau, *Biochem. Pharmacol.*, 2010, **79**, 939-947.

16. N. Hoshi, T. Hirano, T. Omotehara, J. Tokumoto, Y. Umemura, Y. Mantani, T. Tanida, K. Warita, Y. Tabuchi, T. Yokoyama and H. Kitagawa, *Biol. Pharm. Bull.*, 2014, **37**, 1439-1443.

17. L. Gawade, S. S. Dadarkar, R. Husain and M. Gatne, *Food Chem. Toxicol.*, 2013, **51**, 61-70.

18. R. K. S. Devan, P. C. Prabu and S. Panchapakesan, *Drug Chem. Toxicol.*, 2015, **38**, 328-336.

19. W. J. Rea, *J. Nutr. Environ. Med.*, 1996, **6**, 55-124.

20. F. Sánchez-Bayo, *Science*, 2014, **346**, 806-807.

21. J.-L. Brunet, M. Maresca, J. Fantini and L. P. Belzunces, *Toxicol. Appl. Pharmacol*., 2004, **194**, 1-9.

22. C. A. Hallmann, R. P. B. Foppen, C. A. M. van Turnhout, H. de Kroon and E. Jongejans, *Nature*, 2014, **511**, 341-343.

23. M. M. Kandil, C. Trigo, W. C. Koskinen and M. J. Sadowsky, *J. Agric. Food Chem.*, 2015, **63**, 4721-4727.

24. G. J. Rocklin, S. E. Boyce, M. Fischer, I. Fish, D. L. Mobley, B. K. Shoichet and K. A. Dill, *J. Mol. Biol.*, 2013, **425**, 4569-4583.

25. I. Vayá, V. Lhiaubet-Vallet, M. C. Jiménez and M. A. Miranda, *Chem. Soc. Rev.*, 2014, **43**, 4102-4122.

26. S. Tabassum, W. M. Al-Asbahy, M. Afzal, F. Arjmand and R. H. Khan, *Mol. BioSyst.*, 2012, 8, 2424-2433.

27. M. Kallubai, A. Rachamallu, D. P. Yeggoni and R. Subramanyam, *Mol. BioSyst.*, 2015, **11**, 1172-1183.

28. M. H. Tarhoni, T. Lister, D. E. Ray and W. G. Carter, *Biomarkers*, 2008, **13**, 343-363.

29. F. Zsila, *Mol. Pharmaceutics*, 2013, **10**, 1668-1682.

30. L. Brülisauer, G. Valentino, S. Morinaga, K. Cam, J. T. Bukrinski, M. A. Gauthier and J.-C. Leroux, *Angew. Chem. Int. Ed.*, 2014, **53**, 8392-8396.

31. M. A. Williams, in *Protein-Ligand Interactions: Methods and Applications*, ed. M. A. Williams and T. Daviter, Humana Press, New York, NY, 2nd edn., 2013, vol. 1008, pages 3-34.

32. K. Shanmugaraj, S. Anandakumar and M. Ilanchelian, *RSC Adv.*, 2015, **5**, 3930-3940.

33. J. Wang, Q. Li, L. J. Yang, Y. J. Zhang, J. Yu, X. F. Zhao, J. B. Zheng, Y. Y. Zhang and X. H. Zheng, *Anal. Methods*, 2015, **7**, 3340-3346.

34. P. C. Hebert and L. A. MacManus-Spencer, *Anal. Chem.*, 2010, **82**, 6463-6471.

35. C. E. Tinberg, S. D. Khare, J. Y. Dou, L. Doyle, J. W. Nelson, A. Schena, W. Jankowski, C. G. Kalodimos, K. Johnsson, B. L. Stoddard and D. Baker, *Nature*, 2013, **501**, 212-216.

36. K. I. Mikhailopulo, T. S. Serchenya, E. P. Kiseleva, Y. G. Chernov, T. M. Tsvetkova, N. V. Kovganko and O. V. Sviridov, *J. Appl. Spectrosc.*, 2008, **75**, 857-863.

37. Y.-q. Wang, B.-p. Tang, H.-m. Zhang, Q.-h. Zhou and G.-c. Zhang, *J. Photochem. Photobiol. B: Biol.*, 2009, **94**, 183-190.

38. F. Ding, W. Peng, J.-X. Diao, L. Zhang and Y. Sun, *J. Agric. Food Chem.*, 2013, **61**, 4497-4505.

39. F. Ding and W. Peng, *J. Photochem. Photobiol. B: Biol.*, 2015, **147**, 24-36.

40. O. H. Lowry, N. J. Rosebrough, A. L. Farr and R. J. Randall, *J. Biol. Chem.*, 1951, **193**, 265-275.

41. S. Sugio, A. Kashima, S. Mochizuki, M. Noda and K. Kobayashi, *Protein Eng.*, 1999, **12**, 439-446.

42. A. Jakalian, D. B. Jack and C. I. Bayly, *J. Comput. Chem.*, 2002, **23**, 1623-1641.

43. M. Ihara, T. Okajima, A. Yamashita, T. Oda, T. Asano, M. Matsui, D. B. Sattelle

and K. Matsuda, *Mol. Pharmacol.*, 2014, **86**, 736-746.

44. G. M. Morris, R. Huey, W. Lindstrom, M. F. Sanner, R. K. Belew, D. S. Goodsell and A. J. Olson, *J. Comput. Chem.*, 2009, **30**, 2785-2791.
45. G. M. Morris, D. S. Goodsell, R. S. Halliday, R. Huey, W. E. Hart, R. K. Belew and A. J. Olson, *J. Comput. Chem.*, 1998, **19**, 1639-1662.
46. S. Pronk, S. Páll, R. Schulz, P. Larsson, P. Bjelkmar, R. Apostolov, M. R. Shirts, J. C. Smith, P. M. Kasson, D. van der Spoel, B. Hess and E. Lindahl, *Bioinformatics*, 2013, **29**, 845-854.
47. L. D. Schuler, X. Daura and W. F. van Gunsteren, *J. Comput. Chem.*, 2001, **22**, 1205-1218.
48. A. W. Schüttelkopf and D. M. F. van Aalten, *Acta Crystallogr. Sect. D: Biol. Crystallogr.*, 2004, **60**, 1355-1363.
49. W. L. Jorgensen, J. Chandrasekhar, J. D. Madura, R. W. Impey and M. L. Klein, *J. Chem. Phys.*, 1983, **79**, 926-935.
50. H. J. C. Berendsen, J. P. M. Postma, W. F. van Gunsteren, A. DiNola and J. R. Haak, *J. Chem. Phys.*, 1984, **81**, 3684-3690.
51. A. D. Nola, H. J. C. Berendsen and O. Edholm, *Macromolecules*, 1984, **17**, 2044-2050.
52. R. Edberg, D. J. Evans and G. P. Morriss, *J. Chem. Phys.*, 1986, **84**, 6933-6939.
53. A. Baranyai and D. J. Evans, *Mol. Phys.*, 1990, **70**, 53-63.
54. B. Hess, H. Bekker, H. J. C. Berendsen and J. G. E. M. Fraaije, *J. Comput. Chem.*, 1997, **18**, 1463-1472.

55. T. Darden, D. York and L. Pedersen, *J. Chem. Phys.*, 1993, **98**, 10089-10092.

56. T. Darden, L. Perera, L. P. Li and L. Pedersen, *Structure*, 1999, **7**, R55-R60.

57. J. A. Snyman, *Practical Mathematical Optimization: An Introduction to Basic Optimization Theory and Classical and New Gradient-Based Algorithms*, Springer Science＋Business Media, New York, NY, 2005.

58. M. R. Hestenes and E. Stiefel, *J. Res. Natl. Bur. Stand.*, 1952, **49**, 409-436.

59. W. Humphrey, A. Dalke and K. Schulten, *J. Mol. Graph.*, 1996, **14**, 33-38.

60. W. Kabsch and C. Sander, *Biopolymers*, 1983, **22**, 2577-2637.

61. W. G. Touw, C. Baakman, J. Black, T. A. H. te Beek, E. Krieger, R. P. Joosten and G. Vriend, *Nucleic Acids Res.*, 2015, **43**, D364-D368.

62. M. R. Shirts and D. L. Mobley, in *Biomolecular Simulations: Methods and Protocols*, ed. L. Monticelli and E. Salonen, Humana Press, New York, NY, 2013, vol. 924, pp 271-311.

63. J. E. Kerrigan, in *In Silico Models for Drug Discovery*, ed. S. Kortagere, Humana Press, New York, NY, 2013, vol. 993, pp 95-113.

64. J. Weiser, P. S. Shenkin and W. C. Still, *J. Comput. Chem.*, 1999, **20**, 217-230.

65. M. R. Eftink, in *Topics in Fluorescence Spectroscopy: Protein Fluorescence*, ed. J. R. Lakowicz, Kluwer Academic Publishers, New York, NY, 2002, vol. 6, pp 1-15.

66. M. Zolfagharzadeh, M. Pirouzi, A. Asoodeh, M. R. Saberi and J. Chamani, *J. Biomol. Struct. Dyn.*, 2014, **32**, 1936-1952.

67. L. Bekale, P. Chanphai, S. Sanyakamdhorn, D. Agudelo and H. A. Tajmir-Riahi, *RSC Adv.*, 2014, **4**, 31084-31093.

68. O. J. Rolinski, A. Martin and D. J. S. Birch, *Ann. N. Y. Acad. Sci.*, 2008, **1130**, 314-319.

69. L. Brancaleon, *Adv. Protein Chem. Struct. Biol.*, 2013, **93**, 95-152.

70. J. M. Beechem and L. Brand, *Annu. Rev. Biochem.*, 1985, **54**, 43-71.

71. S. L. C. Moors, A. Jonckheer, M. D. Maeyer, Y. Engelborghs and A. Ceulemans, *Curr. Protein Pept. Sci.*, 2008, **9**, 427-446.

72. O. K. Abou-Zied, N. Al-Lawatia, M. Elstner and T. B. Steinbrecher, *J. Phys. Chem. B*, 2013, **117**, 1062-1074.

73. S. Agatonovic-Kustrin, D. W. Morton, L. Truong and S. Razic, *Comb. Chem. High Throughput Screen.*, 2014, **17**, 879-890.

74. C. Dufour and O. Dangles, *Biochim. Biophys. Acta – Gen. Subj.*, 2005, **1721**, 164-173.

75. N. A. Kratochwil, W. Huber, F. Müller, M. Kansy and P. R. Gerber, *Biochem. Pharmacol.*, 2002, **64**, 1355-1374.

76. P. Sevilla, J. M. Rivas, F. García-Blanco, J. V. García-Ramos and S. Sánchez-Cortés, *Biochim. Biophys. Acta – Proteins Proteomics*, 2007, **1774**, 1359-1369.

77. H. N. Bischel, L. A. MacManus-Spencer and R. G. Luthy, *Environ. Sci. Technol.*, 2010, **44**, 5263-5269.

78. A. Bolli, M. Marino, G. Rimbach, G. Fanali, M. Fasano and P. Ascenzi, *Biochem. Biophys. Res. Commun.*, 2010, **398**, 444-449.

79. E. J. Olson and P. Bühlmann, *J. Org. Chem.*, 2011, **76**, 8406-8412.

80. J. B. F. Lloyd, *Nat. Phys. Sci.*, 1971, **231**, 64-65.

81. J. N. Miller, *Analyst*, 1984, **109**, 191-198.

82. E. A. Burstein, N. S. Vedenkina and M. N. Ivkova, *Photochem. Photobiol.*, 1973, **18**, 263-279.

83. N. J. Greenfield, *Methods Enzymol.*, 2004, **383**, 282-317.

84. A. J. S. Jones, *Adv. Drug Deliv. Rev.*, 1993, **10**, 29-90.

85. F. R. N. Gurd and T. M. Rothgeb, *Adv. Protein Chem.*, 1979, **33**, 73-165.

86. A. D. Vogt and E. D. Cera, *Biochemistry*, 2013, **52**, 5723-5729.

87. X. M. He and D. C. Carter, *Nature*, 1992, **358**, 209-215.

88. A. Cavalli, A. Spitaleri, G. Saladino and F. L. Gervasio, *Acc. Chem. Res.*, 2015, **48**, 277-285.

89. R. Buonfiglio, M. Recanatini and M. Masetti, *ChemMedChem*, 2015, **10**, 1141-1148.

90. J. Wereszczynski and J. A. McCammon, *Q. Rev. Biophys.*, 2012, **45**, 1-25.

91. I. Slynko, M. Scharfe, T. Rumpf, J. Eib, E. Metzger, R. Schüle, M. Jung and W. Sippl, *J. Chem. Inf. Model.*, 2014, **54**, 138-150.

92. M. Lundborg and E. Lindahl, *J. Phys. Chem. B*, 2015, **119**, 810-823.

93. K. A. Ford and J. E. Casida, *Chem. Res. Toxicol*., 2006, **19**, 944-951.

94. M. Tomizawa, D. Maltby, T. T. Talley, K. A. Durkin, K. F. Medzihradszky, A. L. Burlingame, P. Taylor and J. E. Casida, *Proc. Natl. Acad. Sci. U. S. A.*, 2008, 105, 1728-1732.

95. http://www.vega-qsar.eu/

96. http://www.epa.gov/opptintr/exposure/pubs/episuite.htm

97. http://www.epa.gov/nrmrl/std/qsar/qsar.html

98. E. Taillebois, Z. Alamiddine, C. Brazier, J. Graton, A. D. Laurent, S. H. Thany and J.-Y. Le Questel, *Bioorg. Med. Chem.*, 2015, **23**, 1540-1550.

99. http://www2.epa.gov/sites/production/files/documents/rmpp_6thed_final_lowresopt.pdf

100. S. Mondal, R. C. Ghosh, M. Mate and C. K. Ghosh, *Environ. Ecol*., 2009, **27**, 1767-1769.

101. J. Kimura-Kuroda, Y. Komuta, Y. Kuroda, M. Hayashi and H. Kawano, *PLoS ONE*, 2012, **7**, e32432.

102. M. Tomizawa, *Adv. Insect Physiol.*, 2013, **44**, 63-99.

103. L. P. Sheets, A. A. Li, D. J. Minnema, R. H. Collier, M. R. Creek and R. C. Peffer, *Crit. Rev. Toxicol.*, 2015, DOI: 10.3109/10408444.2015.1090948.

104. J. E. Casida, *Environ. Health Perspect.*, 2012, **120**, 487-493.

Table 1
Fluorescence lifetime of albumin as a function of concentrations of imidacloprid

Samples	τ_1 (ns)	τ_2 (ns)	A_1	A_2	τ (ns)	χ^2
Free albumin	3.14	7.18	0.31	0.69	5.93	1.09
Albumin＋imidacloprid (1：1)	3.02	7.02	0.29	0.71	5.86	1.01
Albumin＋imidacloprid (1：2)	2.75	6.73	0.26	0.74	5.70	1.15
Albumin＋imidacloprid (1：4)	2.41	6.31	0.21	0.79	5.49	1.03

Table 2
Stern-Volmer quenching constants and association constants for the conjugation of imidacloprid with albumin at different temperatures

T	c(imidacloprid)$\leqslant$10 μM					c(imidacloprid)$>$10 μM				
(K)	K_{SV} ($\times10^4$ M^{-1})	R^a	K ($\times10^4$ M^{-1})	n	R^a	K_{SV} ($\times10^4$ M^{-1})	R^a	K ($\times10^4$ M^{-1})	n	R^a
298	5.005	0.9853	1.442	0.90	0.9995	8.647	0.9813	116.9	1.27	0.9975
304	4.227	0.9887	0.5559	0.83	0.9996	8.146	0.9962	19.50	1.12	0.9956
310	3.491	0.9946	0.4989	0.83	0.9961	6.457	0.9821	9.977	1.08	0.9973

[a] R is the correlation coefficient.

Table 3
Secondary structure assignment of native and mutated albumin allocated via DSSP method

Samples	Secondary structure elements (%)			RMSD (nm)	
	α-Helix	β-Sheet	Turn	Backbone	Ligand
Albumin	54.1	10.3	10.7	0.305	—
Albumin＋imidacloprid	44.3	12.7	13.5	0.352	0.086
Albumin＋thiacloprid	43.5	13.8	14.1	0.337	0.112
Albumin＋nitenpyram	48.2	15.6	11.8	0.321	0.144
Albumin＋acetamiprid	46.1	14.2	12.2	0.346	0.108
Albumin (Trp-214→Ala-214)＋imidacloprid	41.8	13.3	15.6	0.409	0.095
Albumin (Phe-211→Ala-211)＋imidacloprid	44.0	11.9	14.2	0.363	0.201
Albumin (Arg-222→Ala-222)＋imidacloprid	42.7	15.1	12.8	0.339	0.114

Table 4
The decomposition of free energies (kcal mol^{-1}) for the albumin-neonicotinoids conjugates through the Molecular Mechanics/Generalized Born Surface Area (MM/GBSA) approach

Systems	ΔE_{ele}	ΔE_{vdW}	$-T\Delta S$	ΔG_{SA}	ΔG_{GB}	ΔG_{bind}	ΔG_{bind} (docking)
Albumin＋imidacloprid	−36.32±0.27	−22.91±0.12	16.39±0.11	−3.44±0.05	38.15±0.57	−6.13	−5.87
Albumin＋thiacloprid	−33.41±0.15	−21.08±0.03	15.57±0.78	−4.61±0.03	35.31±1.06	−4.22	−5.13
Albumin＋nitenpyram	−40.73±0.33	−23.15±0.27	23.21±1.21	−3.08±0.10	36.51±0.63	−7.24	−6.69
Albumin＋acetamiprid	−37.94±0.29	−23.63±0.06	21.02±1.17	−2.77±0.04	36.60±0.52	−6.50	−6.11
Albumin (Trp-214→Ala-214)＋imidacloprid	−34.22±0.21	−20.02±0.05	14.99±0.38	−3.13±0.04	36.68±0.25	−5.70	−5.28
Albumin (Phe-211→Ala-211)＋imidacloprid	−34.37±0.19	−19.30±0.13	18.27±0.24	−3.06±0.10	33.14±0.39	−5.32	−4.99
Albumin (Arg-222→Ala-222)＋imidacloprid	−31.48±0.12	−21.36±0.48	18.45±0.21	−3.50±0.22	31.88±0.46	−6.01	−5.54

Table 5
Biochemical parameters of neonicotinoids reckoned based on quantitative structure-activity relationship

Biochemical parameters	Neonicotinoids			
	Imidacloprid	Nitenpyram	Acetamiprid	Thiacloprid
logK_{ow} (293 K)[a]	(0.57)[h]	(−0.66)[h]	(0.80)[h]	(1.26)[h]
Carcinogenicity[b]	Non-carcinogen	Carcinogen	Carcinogen	Carcinogen
Developmental toxicity[c]	Developmental toxicant	Developmental toxicant	Developmental non-toxicant	Developmental non-toxicant
Fathead minnow LC_{50} (96 h) (mg L^{-1})[d]	108.89	71.47	27.64	4.13
Mutagenicity[e]	Positive	Positive	Positive	Positive
Oral rat LD_{50} (mg kg^{-1})[f]	369.01 (409.93)[h]	954.59 (1576.04)[h]	678.93	1232.67 (444.32)[h]
Ready biodegradability[g]	Non ready biodegradable	Non ready biodegradable	Non ready biodegradable	Non ready biodegradable

[a] From Estimation Program Interface (EPI) Suite.
[b,d,g] From VEGA.
[c,e,f] From Toxicity Estimation Software Tool (TEST), Consensus method.
[h] Experimental data from Estimation Program Interface (EPI) Suite and Toxicity Estimation Software Tool (TEST), respectively.

Graphic for Table of Contents

Both the flexibility of ligand structures and the property of substituents in neonicotinoids play a pivotal role in the functional protein-neonicotinoids recognitions, and this kind of biointeraction may possess great impacts on the collectively potential toxicity of these widely used agrochemicals.

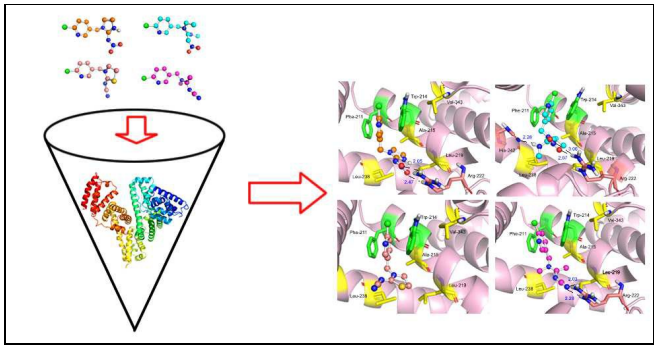

Figure Captions:

Fig. 1. Molecular structures of imidacloprid (A), thiacloprid (B), nitenpyram (C) and acetamiprid (D).

Fig. 2. Fluorescence emission spectra of albumin (1.0 μM) at λ_{ex}=295 nm in the presence of different concentrations of imidacloprid. *c*(imidacloprid)=0, 2.0, 4.0, 6.0, 8.0, 10, 12, 14, 16 and 18 μM (a→j), (x) 18 μM imidacloprid only; pH=7.4, *T*=298 K. The insert shows fluorescence quenching extent of albumin, plotted as extinction of intensity (F/F_0) *against* imidacloprid concentrations correspond to the fluorescence emission spectra. All data were corrected for imidacloprid fluorescence and each point was the mean of three independent observations±S.D. ranging 1.07%～4.39%.

Fig. 3. Stern-Volmer plot describing fluorescence quenching of albumin (1.0 μM) at pH=7.4 in the presence of different concentrations of imidacloprid. Fluorescence intensity was read at λ_{ex}=295 nm, and the emission maximum occurred at 338 nm. Each data was the average of three separate determinations±S.D. ranging 0.25%～4.69%.

Fig. 4. Job's plot for albumin-imidacloprid fluorescence based on the method of continuous variation (pH=7.4, *T*=298 K). All data were corrected for imidacloprid fluorescence and each point was the mean of three respective measurements±S.D.

ranging 0.13%～4.99%.

Fig. 5. Synchronous fluorescence intensity of albumin (1.0 μM) at pH＝7.4, T＝298 K, plotted as extinction of albumin Tyr and Trp residues (F/F_0) *versus* imidacloprid concentration. Each data was the mean of three autonomous detections±S.D. ranging 0.46%～2.86%.

Fig. 6. Superposition of the molecular docking results. Albumin showed in surface colored in light pink, and the ball-and-stick model displays neonicotinoids, colored as per the atoms; (A) orange and blue stick model exhibits the optimal skeletal structure of the binding conformation of imidacloprid with the Gasteiger-Hückel partial charges and the AM1-BCC charges, respectively, blue stick model reveals the skeletal structure of the optimal conformation received by using the ligand from crystal structure (entry codes 3WTL) as the initial conformation; (B) wheat and blue stick model indicates the optimal skeletal structure of the binding conformation of thiacloprid with the Gasteiger-Hückel partial charges and the AM1-BCC charges, respectively, blue stick model hints the skeletal structure of the optimal conformation obtained by utilizing the ligand from crystal structure (entry codes 3WTJ) as the initial conformation; (C) cyan stick model suggests the optimal skeletal structure of the binding conformation of nitenpyram with the Gasteiger-Hückel partial charges; and (D) magenta stick model alludes the optimal skeletal structure of the binding conformation of acetamiprid with the Gasteiger-Hückel partial charges; white stick

model depicts the skeletal structures of the two low energy conformations which have the closest energy with the optimal conformation. (For clarification of the references to color in this figure legend, the reader is referred to the web version of the article.)

Fig. 7. Molecular docking of imidacloprid docked to albumin. Albumin displayed in surface colored in light pink, and the ball-and-stick model shows imidacloprid, colored as per the atoms and the key amino acid residues around imidacloprid have been narrated in stick model; salmon stick model implies hydrogen bonds between Arg-222 residue and imidacloprid; green stick model represents π-π stacking between Phe-211 and Trp-214 residues and imidacloprid; yellow stick model describes hydrophobic interactions between Phe-211, Trp-214, Ala-215, Leu-219, Leu-238, Val-343 residues and imidacloprid. (For interpretation of the references to color in this figure legend, the reader is referred to the web version of the article.)

Fig. 8. Molecular docking of imidacloprid docked to mutated albumin (Trp-214→Ala), the ball-and-stick model portrays imidacloprid, colored as per the atoms and critical amino acid residues around imidacloprid have been denoted in stick model; salmon and yellow stick model hints hydrogen bonds and hydrophobic interactions between mutated albumin and imidacloprid, respectively. (For explanation of the references to color in this figure legend, the reader is referred to the web version of the article.)

Fig. 9. Calculated Root-Mean-Square Deviation (RMSD) from the neonicotinoids and the backbone C_α atoms of albumin from MD simulations at temperature of 298 K with respect to their docking results as a function of the simulation time. The red and black, green and olive, cyan and blue, and magenta and pink trajectories illustrate RMSD values for imidacloprid, thiacloprid, acetamiprid, nitenpyram and the backbone C_α atoms of mutated protein, respectively. The wine trajectory expresses RMSD data for the backbone C_α atoms of pure protein.

Fig. 10. Calculated Root-Mean-Square Deviation (RMSD) from the imidacloprid and the backbone C_α atoms of mutated albumin from MD simulations at temperature of 298 K with respect to their docking results as a function of the simulation time. The red and black (Trp-214→Ala), green and olive (Phe-211→Ala), and cyan and blue (Arg-222→Ala) trajectories symbolize RMSD values for imidacloprid and the backbone C_α atoms of mutated protein, respectively.

Fig. 11. Superposition of the mean conformation of MD simulation on the original conformation of molecular docking resulting from mutated albumin-imidacloprid complex. Protein explained in surface colored in blue green (initial) and pink (average), respectively, and the original and average conformations of imidacloprid delivered in cyan and hot pink ball-and-stick model. The green and pink stick model addresses respectively the initial and average conformations of the crucial amino acid residues involved in the mutated albumin-imidacloprid reaction process. (For

interpretation of the references to color in this figure legend, the reader is referred to the web version of the article.)

Fig. 12. Commercial neonicotinoids constituting of three structural components (A, B and C) and the molecular structures of imidacloprid, thiacloprid, nitenpyram and acetamiprid.

Fig. 13. Molecular docking of nitenpyram (A), acetamiprid (B) and thiacloprid (C) docked to albumin. Albumin exhibited in surface colored in light pink, and the ball-and-stick model reveals neonicotinoids, colored as per the atoms and the key amino acid residues around neonicotinoids have been manifested in stick model; salmon stick model discloses hydrogen bonds between Arg-222, His-242 (Panel (A)) and Arg-222 (Panel (B)) residues and nitenpyram and acetamiprid, respectively; green stick model uncovers π-π stacking between Phe-211 and Trp-214 residues and neonicotinoids; yellow stick model unveils hydrophobic interactions between Phe-211, Trp-214, Ala-215, Leu-219, Leu-238, Val-343 residues and neonicotinoids. (For interpretation of the references to color in this figure legend, the reader is referred to the web version of the article.)

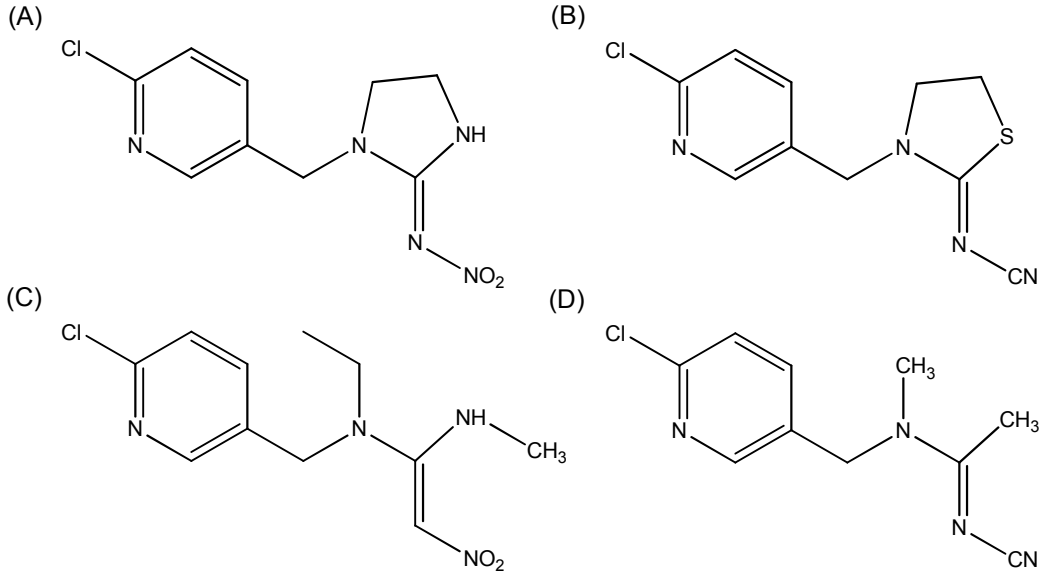

Fig. 1

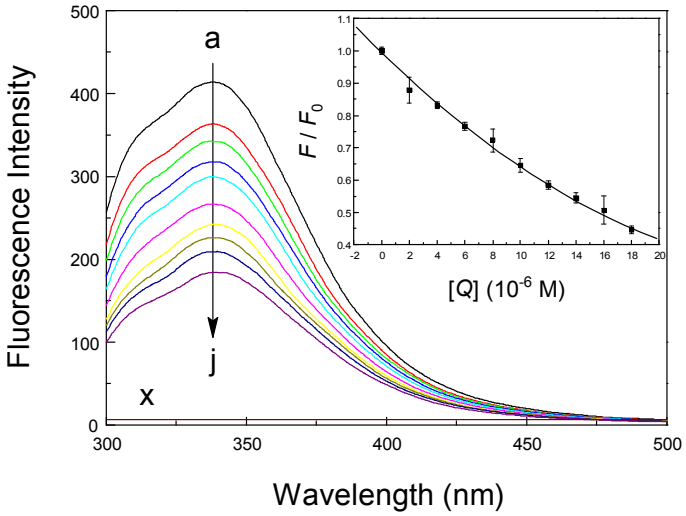

Fig. 2

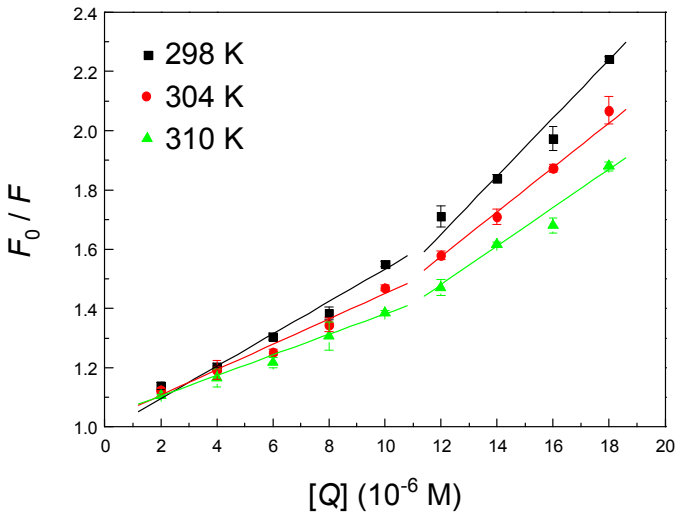

Fig. 3

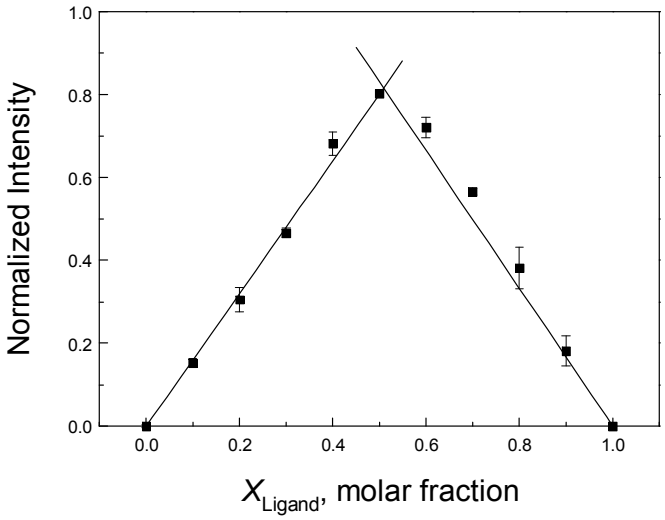

Fig. 4

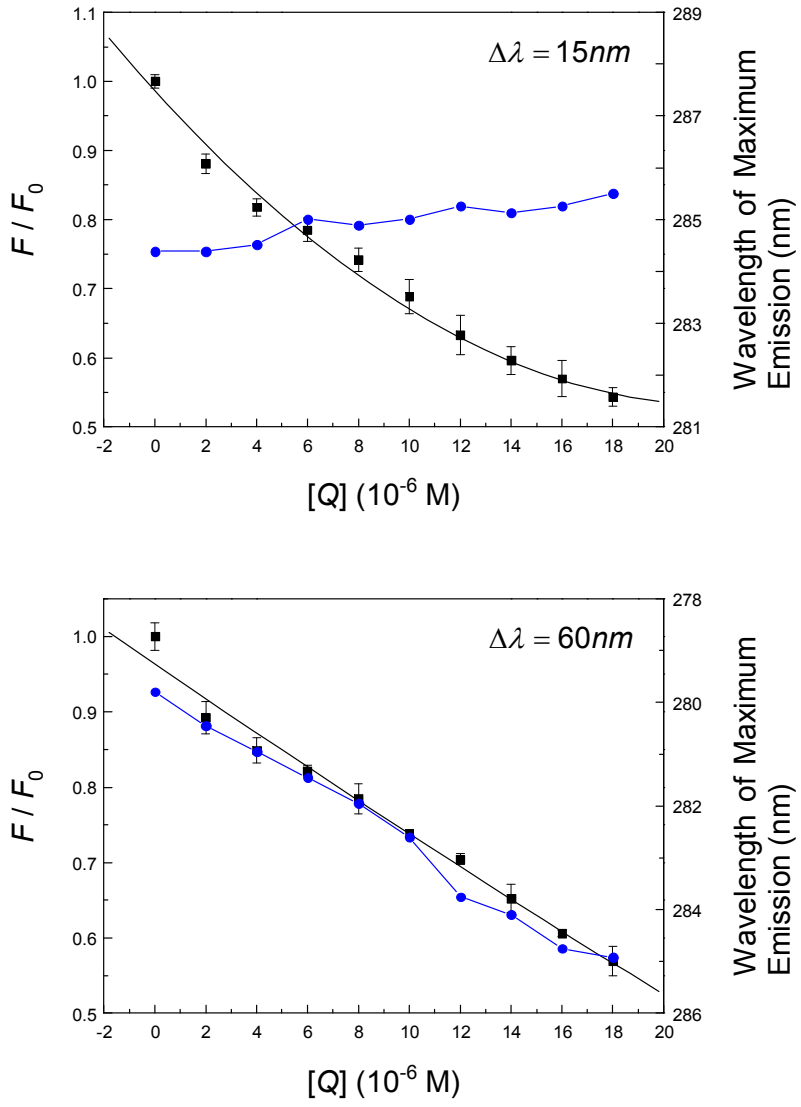

Fig. 5

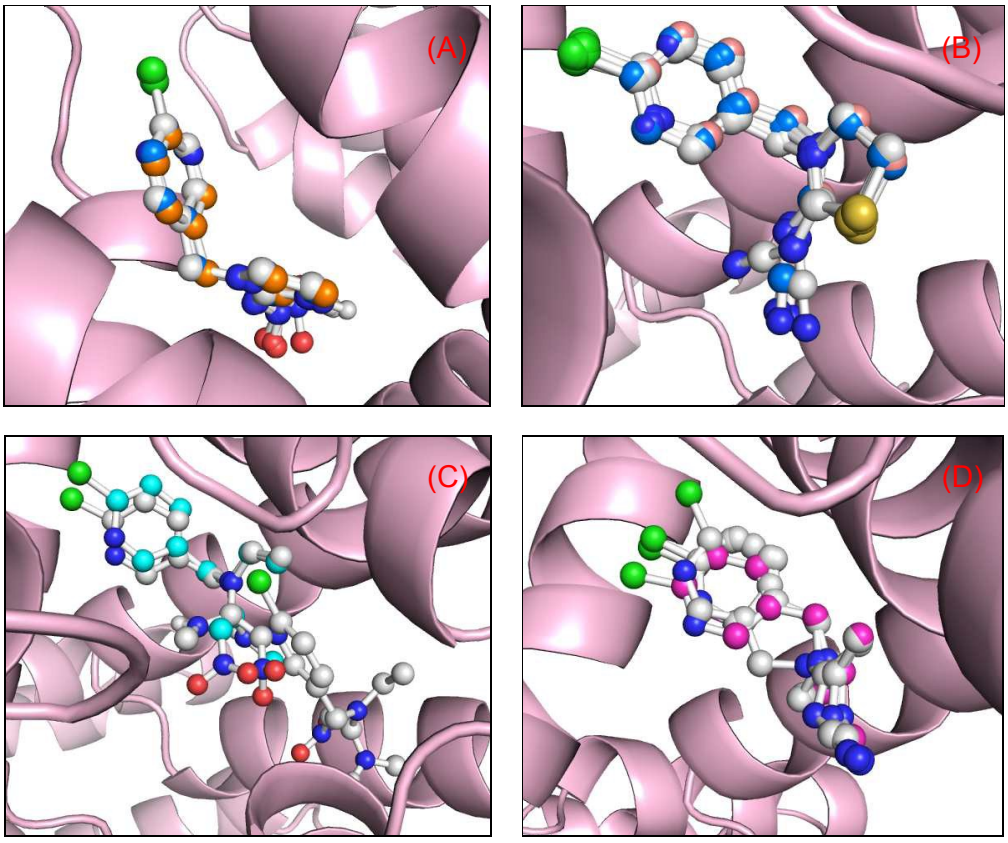

Fig. 6

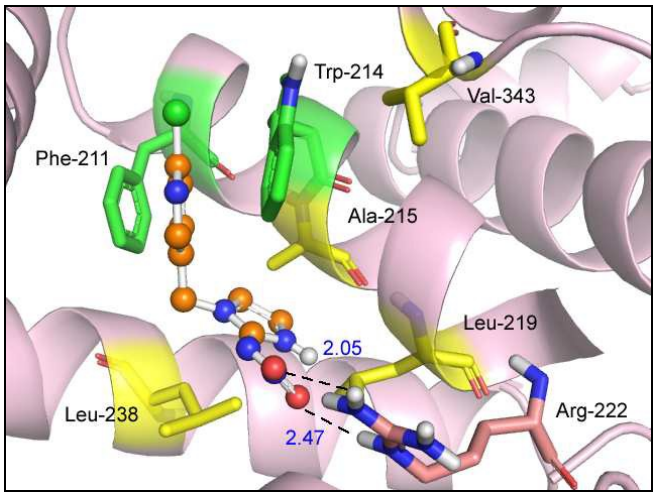

Fig. 7

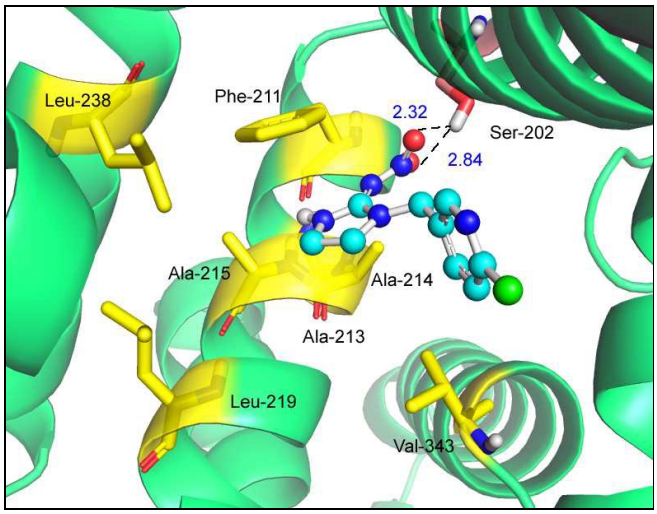

Fig. 8

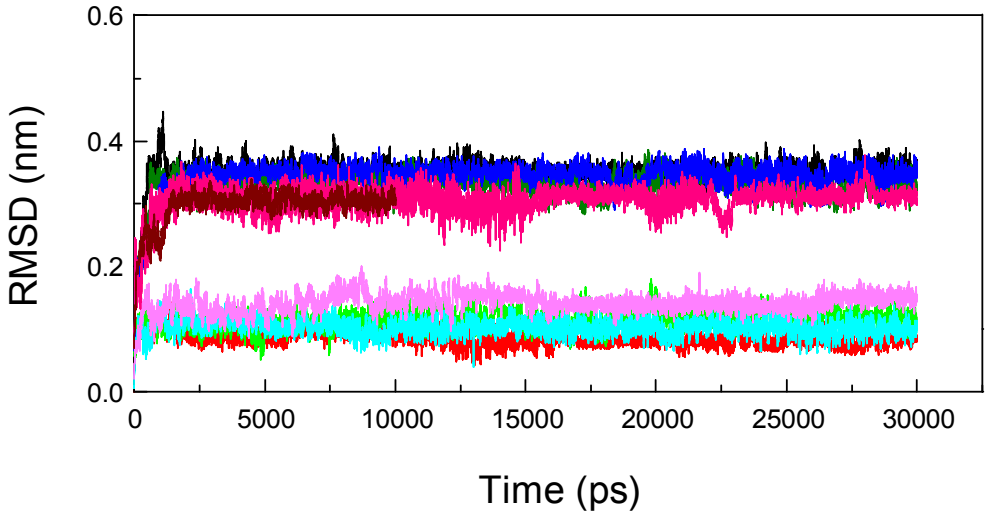

Fig. 9

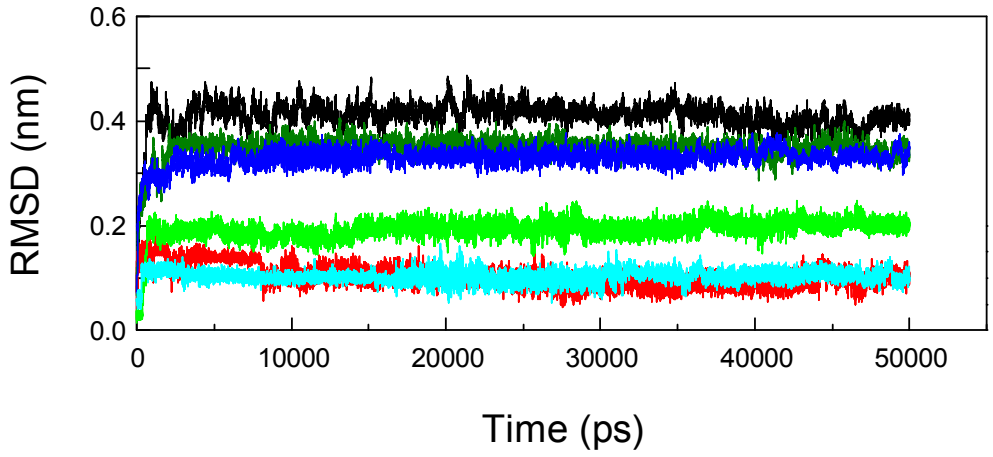

Fig. 10

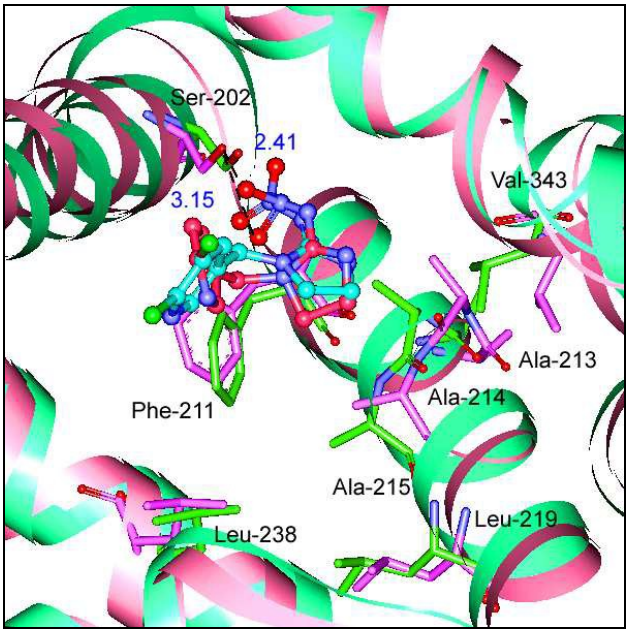

Fig. 11

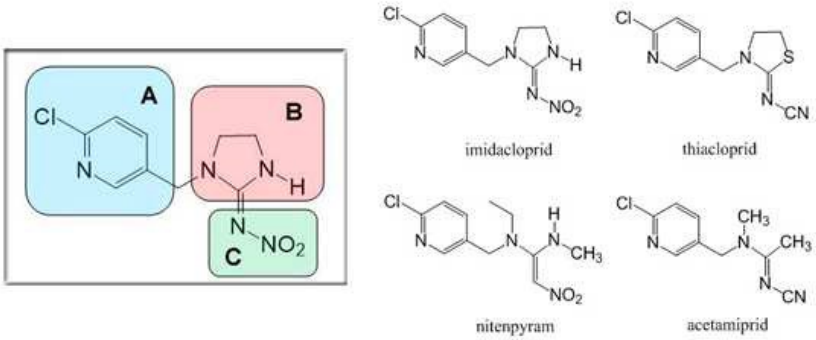

Fig. 12

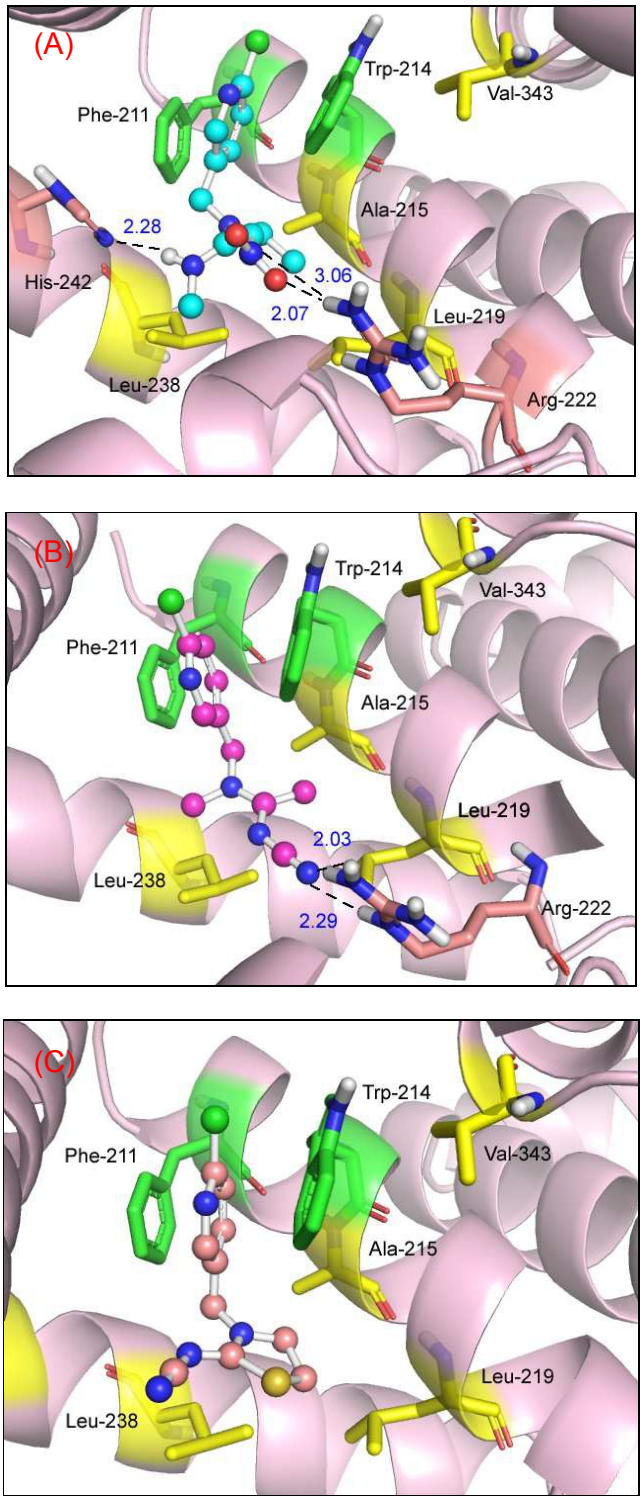

Fig. 13